

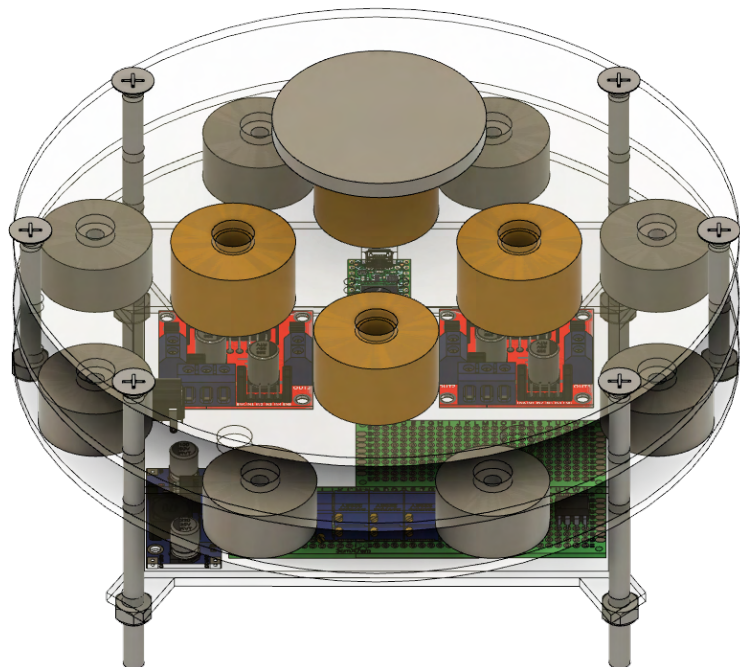
Bachelor's thesis

Martin Brønstad
Jørn Olav Deila
Jørgen Dyrskog
Markus Langklopp

Magnetic levitation system: Design, prototyping and testing of a digital PID-controller

NTNU
Norwegian University of Science and Technology
Faculty of Information Technology and Electrical Engineering
Department of Engineering Cybernetics

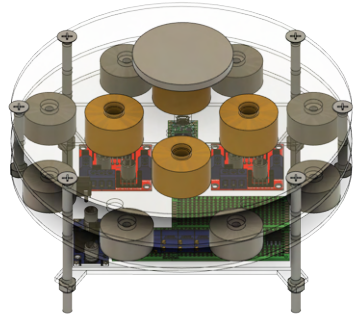
Bachelor's thesis in BIELEKTRO
Supervisor: Christian Fredrik Sætre
May 2022



Norwegian University of
Science and Technology

Martin Brønstad
Jørn Olav Deila
Jørgen Dyrskog
Markus Langklopp

Magnetic levitation system: Design, prototyping and testing of a digital PID-controller



Bachelor's thesis in BIELEKTRO
Supervisor: Christian Fredrik Sætre
May 2022

Norwegian University of Science and Technology
Faculty of Information Technology and Electrical Engineering
Department of Engineering Cybernetics

Task title (English and Norwegian):

Magnetic levitation system: Design, prototyping and testing of a digital PID-controller

Magnetisk levitasjonssystem: Design, prototyping og testing av en digital PID-regulator

Authors: Jørn Deila Jørgen Dyrskog Martin Brønstad Markus Langklopp	Project number: E2207 Submission date: 20.05.2022 Grading: [x] open [] closed
Study: Electrical Engineering - BIELEKTRO	
Study program: Automation and robotics	
Internal supervisor: Christian Fredrik Sætre Department: Department of Engineering Cybernetics	
Client: NTNU ITK Supervisor: Damiano Varagnolo	
Keywords Norwegian: Magnet, magnetic levitation, permanent magnet, neodymium, elektromagnet, magnetisk levitering, PID	Keywords English: Magnet, magnetisk levitasjon, permanent magnet, neodymium, solenoid, levitating, PID

Preface

This bachelor's thesis is written on behalf of the Department of Engineering Cybernetics at the Norwegian University of Science and Technology. The completion of this report marks the end of our three year bachelor's program in electrical engineering with a specialization in automation and robotics.

We would like to thank professor Damiano Varagnolo and PhD Candidate Hans A. Engmark for their continuous help and guidance throughout the project. We would also like to thank Assistant Professor Christian Fredrik Sætre for his assistance and feedback during the project. Finally, we would like to thank the members at Omega workshop for helping us out with the laser cutting.



Martin Brønstad

marbron@stud.ntnu.no



Jørn Olav Deila

jodeila@stud.ntnu.no



Jørgen Dyrskog

jorgedyr@stud.ntnu.no



Markus Langkopp

markla@stud.ntnu.no

Abstract

This bachelor's thesis documents the process of designing, prototyping and building a magnetic levitation platform and controlling the position of a levitating magnet with a digital PID controller.

To achieve this a mathematical framework was developed to describe the system. This framework was based on an existing model of an equivalent analog system, but was expanded to fit the current digital configuration by modelling the new components. The mathematical model was implemented in Matlab and used to simulate the system. This includes analysis of the stability and equilibrium, RGA and condition number analysis, linearization and simulation of a PID-controlled system.

The model and simulations laid the foundation for the design and building of the magnetic levitation platform from scratch. The system was designed with a focus on it being modular and to facilitate various configurations. The process involved designing and cutting modular plexiglass platforms as well as design and construction of an electrical circuit.

Implementation of a digital PID controller was done using a Teensy microcontroller. The control system was designed as a 3x3 MIMO system with three parallel PID controllers. The position of the levitating magnet is measured using hall-effect sensors

When a functional system was built, it was attempted to stabilize the system by tuning the PID controller. In the end the system did not stabilize as anticipated. At best the magnet levitated for no more than 20 seconds before becoming unstable. There has been done a lot of analysis and discussion regarding improvements on the current system. The conclusion is that it is unstable for a number of different reasons, which include the permanent magnetic field, the solenoids themselves, the noise filtering as well as time and budget constraints.

Sammendrag

Denne bacheloroppgaven handler om design, utvikling og bygging av en magnetisk levitasjonsplattform samt posisjonsregulering av en leviterende magnet ved hjelp av en digital PID-regulator.

For å oppnå dette har en matematisk modell blitt utviklet for å beskrive systemet. Modellen er basert på en eksisterende modell av et ekvivalent analogt system som har blitt utvidet til å beskrive det nye, digitale systemet. For å tilpasse den nye modellen måtte de nye komponentene modelleres. Modellen har også blitt implementert i Matlab og har blitt brukt til å simulere systemet. Dette inkluderer analyse av stabilitet og likevektpunkt, RGA- og kondisjonstallanalyse, linearisering og simulering av et PID-regulert system.

Modellen og simuleringene ligger til grunn for designet og byggingen av den nye magnetiske levitasjonsplattformen. Systemet ble designet med tanke på at det skulle være modulært, hvor forskjellige magnetkonfigurasjoner enkelt kunne testes ut. Designprosessen innebar design og kutting av modulære pleksiglassplater samt design og oppkobling av en elektrisk krets.

Implementeringen av den digitale PID-regulatoren ble gjort på en Teensy mikrokontroller. Reguleringssystemet ble designet som et 3x3 MIMO-system med tre PID-regulatorer i parallel. Posisjonen til den svevende magneten blir målt ved bruk av hall-effekt-sensorer.

Når et funksjonelt system var bygget ble det forsøkt stabilisert ved å justere inn PID-regulatoren. Dessverre ble systemet aldri stabilt, og regulatoren klarte ikke holde den svevende magneten i lufta i mer enn 20 sekunder på det meste. Etter mye analyse og diskusjon av det nåværende systemet er konklusjonen at det er mange grunner til at systemet ikke ble stabilt, blant annet det permanente magnetfeltet, elektromagnetene, støyfiltreringen samt tids- og budsjettrestriksjoner.

Contents

1	Introduction	1
1.1	Background	1
1.2	Thesis statement	2
1.3	Structure of the report	3
2	Method	4
2.1	Project management	4
2.1.1	Resources and budget	4
2.2	Hardware and software	5
2.2.1	Hardware	5
2.2.2	Software	6
3	Theoretical framework	7
3.1	Magnetic field laws	7
3.1.1	Earnshaw's theorem	7
3.1.2	Biot-Savart's law	7
3.1.3	Laplace's force law	8
3.1.4	Permanent magnet	8
3.1.5	Solenoids	9
3.1.6	Magnetic permeability	9
3.2	Electronics	10
3.2.1	Hall effect sensor	10
3.2.2	Potentiometer	10
3.2.3	Operation amplifier	11
3.2.4	Instrumentation amplifier	11
3.2.5	Buck converter	12
3.3	Microcontroller	13
3.3.1	Analog- and digital signals	13
3.3.2	PWM-signals	14
3.3.3	ADC	14
3.4	PID-controller	15

3.4.1	Proportional	15
3.4.2	Integral	15
3.4.3	Derivative	16
4	Mathematical model and simulation	17
4.1	System description	17
4.2	Mathematical model	18
4.2.1	Measurements	18
4.2.2	Equilibrium	20
4.3	Matlab implementation	21
4.3.1	Class definition	21
4.3.2	Accurate and fast simulations	22
4.3.3	Z-graph	22
4.4	Modelling the physical components	23
4.4.1	Neodymium magnets	24
4.4.2	Levitating magnet	25
4.4.3	Solenoids	26
4.5	Finding a reasonable configuration	26
4.5.1	Permanent magnets	26
4.5.2	Solenoids	27
4.6	Linear analysis	29
4.6.1	Linearization	29
4.6.2	Transfer function matrix	31
4.6.3	Condition number and RGA	32
4.6.4	PID implementation	33
4.7	Discussion	33
4.7.1	Modelling the components	33
4.7.2	Choice of configuration	33
4.7.3	Fast and accurate simulations	33
4.7.4	Verification of the model	34
4.7.5	Controller parameters	34

5 Design	35
5.1 Physical system	35
5.1.1 Testing	35
5.1.2 System housing	37
5.1.3 Laser cutting	38
5.1.4 Mounting of sensors	38
5.2 Electronics	39
5.2.1 Power input	39
5.2.2 Microcontroller	39
5.2.3 Motor drivers	40
5.2.4 Sensors	40
5.2.5 Testing of sensors	41
5.2.6 Instrumental amplifiers	41
5.3 Results	42
5.3.1 Different configurations	43
5.4 Discussion	44
5.4.1 High temperatures	44
5.4.2 Electrical wiring and soldering	44
5.4.3 Soldering	45
5.4.4 Hall effect sensors placement	45
5.4.5 Damage to the levitating magnet	45
5.4.6 System modularity	46
5.4.7 Number of sensors	46
5.4.8 Component replacements	47
5.4.9 Solenoid core material	47
5.4.10 Noise generated by the solenoids	47
6 Controller design	49
6.1 Choice of control structure	49
6.2 Digital PID-design	50
6.2.1 Position form	50
6.2.2 Incremental form	51

6.2.3	Tuning the PID-controller	52
6.3	Microcontroller settings	53
6.3.1	ADC	53
6.3.2	PWM	53
6.4	Sensor readings	54
6.4.1	Noise analysis	55
6.4.2	Filter design	56
6.5	Output algorithm	56
6.6	Discussion	58
6.6.1	Stabilisation issues	58
6.6.2	Output algorithm	60
6.6.3	Permanent magnetic field	63
6.6.4	Two dimensional control	63
6.6.5	State observer	64
7	Results	65
8	Discussion	66
8.1	Future work	66
9	Conclusion	67
Attachments		71
A	Plexi-glass design in Inkscape	71
B	Plexi-glass design in Fusion360	72
C	Sources for used 3D assets in Fusion360	73
D	Electrical schematic, landscape	74
E	Teensy Pinout	75
F	Matlab parameters	76

G Linearized system matrices**77****H Poster****78**

List of Figures

1.1	The analog system	2
3.1	Illustration of the magnetic field generated by a permanent magnet	8
3.2	Illustration of a solenoid and its magnetic field (Chegg no date)	9
3.3	Illustration of a hall effect sensor (ElectronicsTutorial no date)	10
3.4	Diagram and insides of a trimpot	11
3.5	Operational amplifier circuits	12
3.6	Illustration of an instrumentation Amplifier ((WikimediaCommons 2009b))	13
3.7	Illustration of PWM signals made in diagrams.net	14
4.1	System illustration with coordinate frame. The origin is aligned with the top of the permanent magnets.	17
4.2	Top and side view of a solenoid modelled with the two different methods. This example has $nr = 5$ and $nh = 5$	22
4.3	Example of a z-graph. The z-position of the levitating magnet z_m is on the x-axis.	23
4.4	Measuring levitating height between two stacks of three neodymium magnets	24
4.5	Z-graph for four different permanent magnet configurations	27
4.6	Force in x-direction with no current vs max current in solenoids	28
4.7	Force in x-direction with solenoids placed at $z_s = 0$ vs $z_s = 0.023$	29
4.8	Comparison of simulated permanent magnetic fields	34
5.1	Testing magnet distances with the analog system	36
5.2	Testing the maximum current	36
5.3	Electrical housing	37
5.4	Measurements height	38
5.5	Hall effect sensors epoxied on the sensor-board	39
5.6	Comparison between the schematic and the physical implementation	42
5.7	Different angles of the finished physical system	43
5.8	Different configurations	44
5.9	Close soldering	45
5.10	Damages on the levitating magnet	46
6.1	Block diagram control structure	49
6.2	ADC analysis with averaging set to 4	54

6.3	Filter analysis	56
6.4	Output logic in a flow diagram	58
6.5	Bit manipulation	59
6.6	On/off control of the solenoids	59
6.7	Output values from the Teensy 3.5 seconds to 4.0 seconds, plotted in Python	60
6.8	Step response of the solenoid	61
6.9	Simulated actual current in the solenoids [A].	62
6.10	Comparison of simulated permanent magnetic fields	64
7.1	Different angles of the finished physical system	65

List of Tables

2.1	List of components and costs in NOK	5
4.1	Specifications for a stack of three neodymium magnets	25
4.2	Specifications for the levitating magnet	25
4.3	Specifications for the solenoids	26
6.1	PID parameters after tuning	53
6.2	Output saturations	57
6.3	Outputs to different solenoids	57

Acronyms

ADC Analog to Digital Converter. 14

DAC Digital to Analog Converter. 14

In-Amp Instrumentation Amplifier. 4, 11, 12, 41

MIMO Multiple-Input Multiple-Output. 49

MSB Most Significant Bit. 14, 15

NOK Norwegian krone. x, 4, 5

Op-Amp Operational Amplifier. 11, 12, 14

PWM Pulse Width Modulation. ix, 14, 40, 53, 54, 57, 58

Definitions

equilibrium The state in which opposing forces are balanced. 7, 50

1 Introduction

1.1 Background

Magnetic levitation is a highly advanced technology used in a variety of different applications. The common thing for magnetic levitation systems is that a part of the system is kept levitated by a magnetic force. As a result these parts get little to no wear and friction because of the lack of contact.

The first magnets were discovered by the Ancient Greeks, when they found the rock magnetite (Binnie 2001). However it was not until 1842 when Samuel Earnshaw proved a theorem regarding magnetic levitation, which turned out to be essential within the field. Earnshaw's theorem shows that it is impossible to achieve stable non-contact levitation between static magnets alone (Yaghoubi 2013). This means that in order to keep a levitating magnet stable, it needs a stabilizing force. This is usually achieved by actively controlling solenoids.

The first major application in which magnetic levitation was used, was in the 1950s. Prior to the 50s when testing airflow around parts of an aeroplane in a wind tunnel, mechanical structures was used to hold the parts still. This however interfered with the measured drag flow of the parts. Then in the 50s a solution was developed by Eugene E. Covert to use magnetic stabilisation to eliminate the interference of the mechanical structure (Yaghoubi 2013). The magnets and instruments were placed outside the test area, and the measurements of drag therefore only consisted of the drag of the parts that were tested.

A more modern and well known application in which magnetic levitation is used, is in so called maglev trains. These trains are widely used in both Japan and Shanghai. This is based on advanced technology of maglev using superconducting magnets. This allows the train to have low to zero friction, beside the air resistance, and therefore allows the trains to reach speeds of above 500 km/h (Ono, Koga and Ohtsuki 2002).

The magnetic levitation platform that is designed and tested in this project, are based on the same principles as the examples above. However, it merely consists of a levitating disc magnet above a base. The main components of the base consists of neodymium permanent magnets, as well as solenoids for stabilization. The most common way of controlling the solenoids, is by implementing an analog PD-controller. Such an analog system is shown in figure 1.1. However, the goal of this project is for the solenoids to be digitally controlled by a microcontroller.

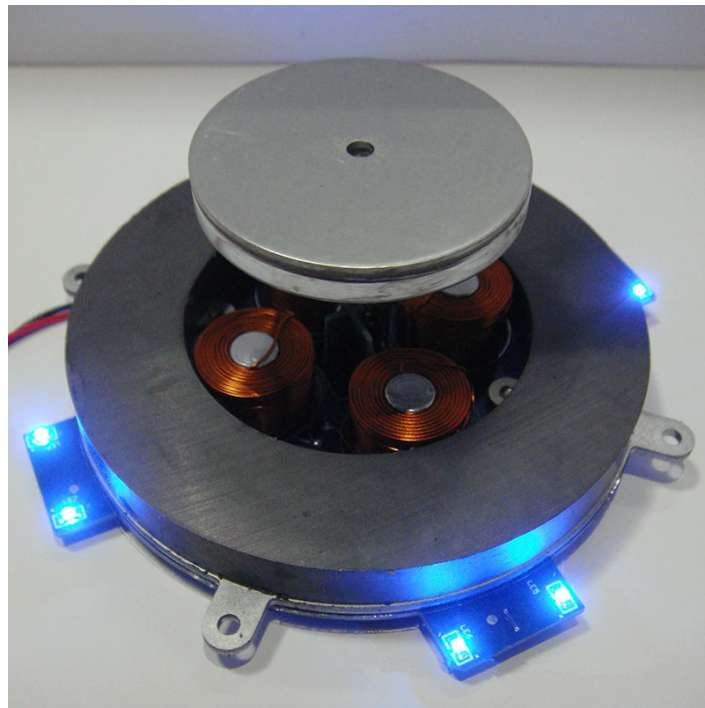


Figure 1.1: The analog system

(AliExpress N.D)

1.2 Thesis statement

The main focus of this project is building a magnetic levitation platform and controlling the position of a levitating magnet digitally. This involves designing a system suitable for control, connecting it to a microcontroller and implementing a PID controller. The finished system is meant to be a proof of concept, to possibly be used as a learning platform at ITK in the future.

Some of the key tasks during the project are expected to be:

- Modelling new components and implementing them into the Matlab model
- Using the Matlab model to simulate different magnet configurations
- Designing the new platform layout using CAD software
- Designing the electrical circuit
- Deciding on a controller structure aided by the mathematical framework
- Implementing, testing and tuning a digital PID-controller

1.3 Structure of the report

The report is split into 9 different main chapters, where each of the chapters contains different information about the project.

The first chapter is an introduction to the subject. This chapter includes background information which is relevant to the task, including information about magnets and different applications in which magnetic levitation has been used. This chapter also contains the thesis statement, as well as an overview over the structure.

The second chapter contains information about the methods used in the project. It includes an overview over the resources and budget for the project, as well as a complete listing of the hardware and software used.

The third chapter is intended to give the theoretical framework needed to understand the subject. This includes relevant theory subjects such as magnetic field, electronics, microcontroller and controllers.

The fourth chapter is the first main chapter about the practical work that has been done regarding the project. This chapter is about the mathematical model and simulations. This includes an introduction to the mathematical model and how this was implemented in Matlab. All relevant simulations and findings in the simulations are shown. There is also an analysis and discussion section, which takes a look at the advantages and disadvantages regarding the modelling and simulation.

The fifth chapter gives an overview over the design phase in the project. This includes the reason for the designs, as well as testing and building of the physical system. It also has information about the electronics used in the system. The two last sections include information about the concrete results that were achieved, as well as a discussion about the choices made and potential improvements.

The sixth chapter is about the design and development of the controllers used in the magnetic levitation platform. It includes information about PID-controllers, why they were selected and the selected control strategy. It also contains information about the digital choices that were made. This includes the choice of different settings on the microcontroller, as well as filtering and output algorithms. Finally it includes a discussion about the choices that were made, and potential improvements regarding control.

The seventh and eight chapters include the main results and discussion about these results. The ninth chapter includes the main conclusion regarding the projects achievements.

2 Method

2.1 Project management

2.1.1 Resources and budget

Due to this thesis having a set time limit, and the fact that some of the components had weeks of shipping time, the preliminary focus was getting the materials and hardware as quickly as possible while maintaining a low cost. Considering the shipping time, it was decided to purchase some spare components in case an accident occur. This includes extra solenoids and neodymium magnets, and extra parts would also come in handy if the design was to be changed during the testing period. The prices below are not completely replicatable, due to the fact that some of the components were bought locally. This means there were no extra VAT or shipping costs for these components.

The total cost of the entire setup with no spare parts, would be approximately 2100 NOK. This does not include the cost for shipping. The total cost could also be reduced by scaling down the system, meaning less neodymium magnets and the number of sensors could be reduced to three. A reduction of sensor would also include a reduction of In-Amps. This would reduce the cost of the entire system by approximately 400 NOK. The original budget was set at approximately 2000 NOK. However, the extra costs above this were approved by the task giver. The final budget ended up on approximately 3700 NOK, as shown in table 2.1.

Components	Amount	Price	Shipping	VAT	Price inc. VAT	Delivery date
8 pc 32x5mm Neodymium magnets with holes	4	501,08	365,16	216,69	717,77	1-2 weeks
5 pc 19mm OD Electromagnets	2	229,26	0,00	56,33	285,59	2-4 weeks
3 pc 35mm OD Solenoids	2	292,68	29,29	80,55	402,52	2-4 weeks
Hall effect	7	98,00	0	0	98,00	Workshop
Motor driver	2	94,00	0	0	94,00	Workshop
Instrumentation Amplifier (In-Amp)	7	210,00	0	0	210,00	Workshop
Plexiglass	1	230,00	0	0	230,00	Workshop
Teensy 4.0	1	300,00	0	0	300,00	Workshop
Power supply 35 W	1	300,00	0	0	300,00	local shop
Repairs and replacements		484,92	120	92,73	577,65	
			Total shipping		Sum price	Total price
			505,45		3218,54	3723,99

Table 2.1: List of components and costs in NOK

2.2 Hardware and software

During the project, different hardware and software was used for project management, simulations, designing, building, testing and development of the magnetic levitation platform. Below is a complete table of all the hardware that was used during the project, as well as a complete list of all the software that was used.

2.2.1 Hardware

1. Lasercutter : Bodor BCL-1309XU
2. Various tools at Omega & Elektra workshops
3. Oscilloscope
4. Variable power supply
5. Resistors
6. Potentiometers
7. Various 0.5 mm² and 0.7 mm² cables

8. Stripboards
9. The hardware mentioned in Table 2.1

2.2.2 Software

1. Microsoft Teams
2. Microsoft Word
3. Microsoft Excel
4. Overleaf
5. Matlab
6. Python
7. Arduino IDE
8. Teensyduino
9. InkScape
10. KiCad
11. GanttProject
12. RD works
13. Fusion 360
14. Diagrams.net (formerly Draw.io)

3 Theoretical framework

The purpose of this chapter is to provide the theoretical framework needed. The chapter includes various theorems and laws that are relevant to the project. It also includes relevant knowledge about components such as magnets, sensors and integrated circuits.

3.1 Magnetic field laws

A magnetic field is a vector field generated by a magnet of some sort. This vector field describes the magnetic influence on moving electric charges, electric currents and magnetic materials. The vector field is in itself complex to simulate and calculate, so this section covers the theoretical framework needed to comprehend this subject.

3.1.1 Earnshaw's theorem

One of the most essential theorems in the magnetic levitation industry, is a theorem presented by Samuel Earnshaw in 1840. The theorem states that "*no system of charged particles can be in stable static equilibrium in the absence of external forces*" (Jones 1980).

This essentially means that it is not possible to keep the levitating magnet stable, only by the static magnetic field from permanent magnets. The levitating magnet needs some form of stabilizing force, which in this project is provided by four solenoids. The goal is therefore to control the solenoids in order to create a stable equilibrium for the levitating magnet.

3.1.2 Biot-Savart's law

Biot-Savart's law is generally an equation that describes the magnetic field generated by a current. More specifically it computes the magnetic field B at a position r in a 3D space, generated by a constant current I :

$$B(r) = \frac{\mu_0}{4\pi} \int_C \frac{Id\ell \times r'}{|r'|^3} \quad (3.1)$$

Where I is the current in a wire, $d\ell$ is a differential vector along the line C (wire), μ_0 is the permeability of air, C is the wire and r' is the point at which the magnetic field is being computed. r' corresponds to $p - \ell$, where p is a point in Cartesian coordinates and ℓ is the point on the line C (wire).

3.1.3 Laplace's force law

Laplace's force law is a law derived from Lorentz force law. Laplace's force law states the net magnetic force on a stationary and rigid curved wire, with a steady current. This is given by

$$F_b = I \int_C d\ell \times B \quad (3.2)$$

Where F_b is the magnetic force, I is the current, $d\ell$ is an infinitesimal segment of the wire C , and B is the magnetic field.

3.1.4 Permanent magnet

A permanent magnet is a magnet in which the magnetic field originates from the internal material of the magnet itself. The magnetic field generated from the magnet is permanent, meaning it can never be turned off as in a solenoid. The magnets used in this project are neodymium magnets, which are made of the alloy of neodymium, iron and boron. This is the strongest type of permanent magnet in the world as of today (Fraden 2010).

The magnetic field from a permanent magnet are most vertical near the poles. A simulation of the magnetic field around a neodymium magnet is shown in figure 3.1. The gray box in the middle is a stack of 3 neodymium magnets, shown from the side. The blue vector field represents a cross section of the magnetic field, shown in the yz -axis.

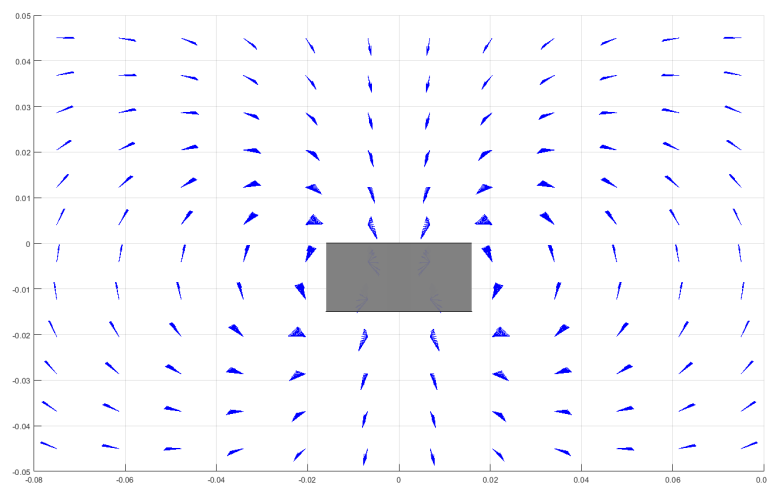


Figure 3.1: Illustration of the magnetic field generated by a permanent magnet

3.1.5 Solenoids

A solenoid is a type of electromagnet. It consists of a coiled cylindrical copper wire, which gets magnetized when current flows through it. The difference between an electromagnet and a solenoid, is the core. An electromagnet has a core of magnetic material, e.g. iron, which becomes magnetized when current flows through the wire. A solenoid has the same coil of wires, but not a core that can be magnetized. Figure 3.2 is an illustration of the magnetic field generated by a current I , flowing through the coil of wire. N and S are the north and south pole of the generated magnetic field.

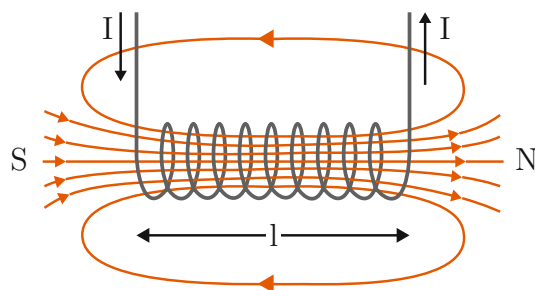


Figure 3.2: Illustration of a solenoid and its magnetic field (Chegg no date)

3.1.6 Magnetic permeability

Magnetic permeability is the physical aspect of the magnetization certain materials obtain when being exposed to a magnetic field. In electromagnetism this has an impact on the strength of the magnetic field, in regards of different materials used in the core. An electromagnet that has a low permeability core has a lower magnetic field strength compared to the same electromagnet with a higher permeability in the core. An example of an electromagnet with a low permeability core is a solenoid, which can use air or plastic in the core. This has a lower magnetic field strength than a coil using an iron- or stainless steel core.

This also has an impact on the inductance. The greater the permeability, the greater the inductance of an electromagnet. This effects the time constant, τ , of the coil. The formula for τ is shown in equation 3.3, and consists of the inductance L divided by the resistance R .

$$\tau = \frac{L}{R} \quad (3.3)$$

The electromagnets τ is the ability for the coils to reach 63% of its applied current. It takes 5τ for the

coils to reach within $\pm 1\%$ of its final value.

3.2 Electronics

The project includes designing and building a magnetic levitation platform from scratch. This section is therefore a theoretical framework needed to understand the electrical components, and their function.

3.2.1 Hall effect sensor

A hall effect sensor is used to measure the strength of a magnetic field. It works by sending an electric current through a conductive plate. When a magnetic force is applied to one of the sides of this plate, a voltage difference appears between the two sides of the plate. This voltage difference appears due to Lorentz force. The voltage difference can then be measured, and is proportional to the strength of the magnetic field applied to the plate. An illustration of a hall effect sensor, which is dependent on a magnet moving towards or away from the sensor, is shown in figure 3A3K. Parkhe et al.

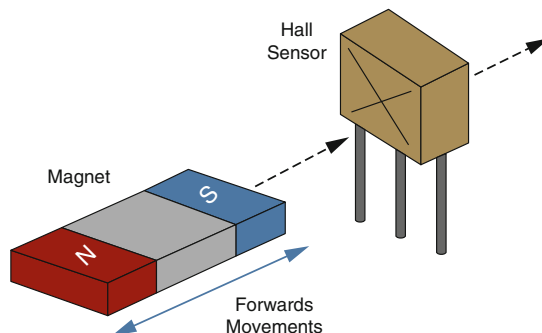
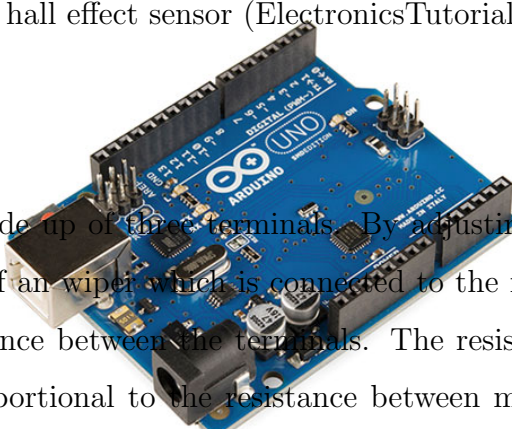


Fig. 2 Principle of Hall Effect Sensor

Figure 3: Illustration of a hall effect sensor (ElectronicsTutorial no date)
Fig. 3 Arduino Uno

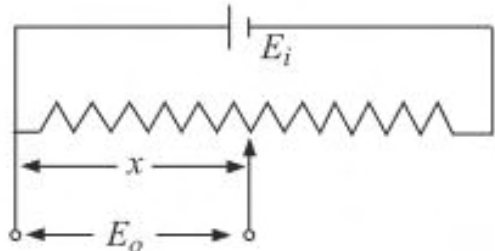
3.2.2 Potentiometer

A potentiometer is a variable resistor made up of three terminals. By adjusting either an rotating or translatory part, it adjusts the position of an wiper which is connected to the middle terminal. When the wiper is moved, it adjusts the resistance between the terminals. The resistance between the first terminal and the middle is inversely proportional to the resistance between middle terminal and the last. There are several types of potentiometers, and the type used in this project is called a multiturn trimpot. A trimpot are more sensitive than traditional potentiometer, and usually is controlled by

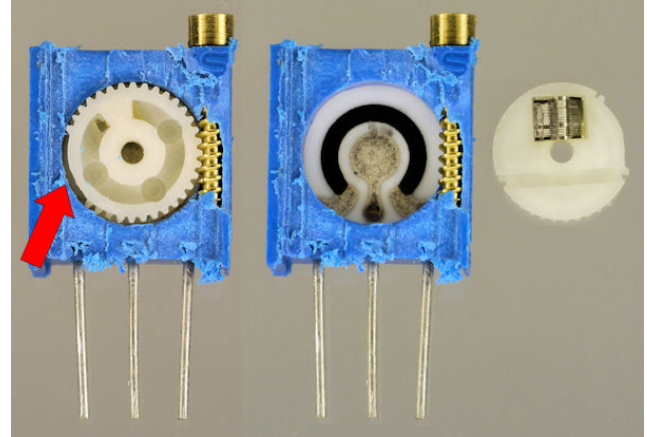


The experimentation has been carried on composite beam by varying load at the free end to find the deflection using Hall Effect sensor. The designed Hall Effect sensor will generate maximum voltage up to 220 volts if the distance between the sensor and the magnet is up to 6 mm. Initially, we put 1–2 mm distance between sensor and

an screw that can be rotated several times to control the resistance. The screw on top is a leadscrew that is connected to the wiper. When the screw is turned, the positioning of the wiper is changed which adjusts the resistance between the terminals. An diagram of an multiturn potentiometer, and a picture of the insides are shown in figure 3.4.



(a) Illustration of an translational potentiometer
(Ghosh 2012)



(b) The insides of a trimpot
(Cook N.D)

Figure 3.4: Diagram and insides of a trimpot

3.2.3 Operation amplifier

An Operational Amplifier (Op-Amp) is an integrated circuit that can amplify weak electric signals (ABLIC no date). The Op-Amp has two inputs, and one output. It uses the difference in voltage between the two inputs, amplifies it and outputs the amplified differential voltage. Depending on the surrounding circuit and configurations the op-amp can serve many different purposes. The differential amplifier and voltage follower are the most relevant configurations for this project. These are shown in figure 3.5.

3.2.4 Instrumentation amplifier

The Instrumentation Amplifier (In-Amp) is a circuit normally built from three Operational Amplifiers. The circuit is shown in figure 3.6, where $R_1 = R_2 = R_3 = R$. This allows for an adjustable amplifying circuit, where the amplification can be adjusted by changing R_{gain} .

The top left Op-Amp is a negative feedback amplifier, so the voltage above R_{gain} is equal to V_1 . The same is for the bottom left Op-Amp, meaning the voltage below R_{gain} equals V_2 . This gives a voltage

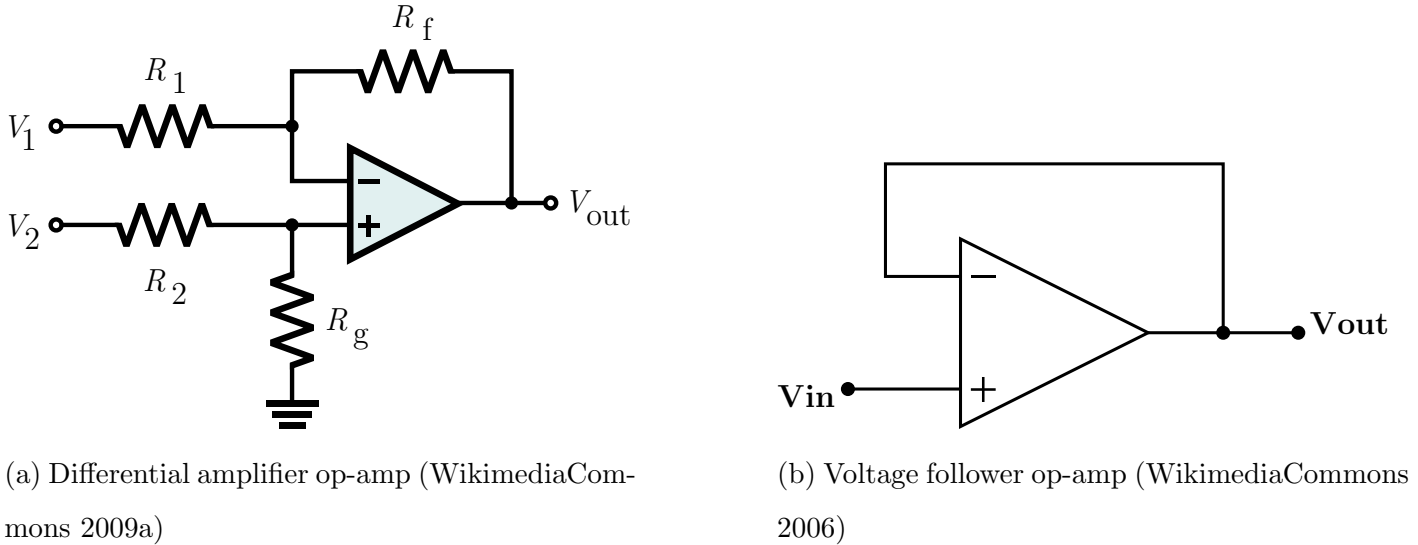


Figure 3.5: Operational amplifier circuits

drop across R_{gain} equal to the difference between V_1 and V_2 . This generates a current through R_{gain} , which in turn generates the following voltage to the left of the upper and lower R_2 :

$$V = (V_2 - V_1)(1 + \frac{2R_1}{R_{gain}}) \quad (3.4)$$

The right Op-Amp is known as a differential amplifier circuit (ABLIC no date), and has the following V_{out} :

$$V_{out} = (V_2 - V_1) \frac{R_3}{R_2} \quad (3.5)$$

Since $R_3 = R_2 = R_1 = R$, the V_{out} of the In-Amp-circuit is:

$$V_{out} = (V_2 - V_1)(1 + \frac{2R}{R_{gain}}) \quad (3.6)$$

3.2.5 Buck converter

A buck converter steps down DC or rectified AC voltage. It usually consists of a switching transistor, a diode, an inductor and a capacitor. While the switch is on, the current charges the capacitor but the voltage is limited by the inductor. When the switch turns off, the diode and the inductor causes the current to flow in the opposite direction. The direction of the current changes thousands of times

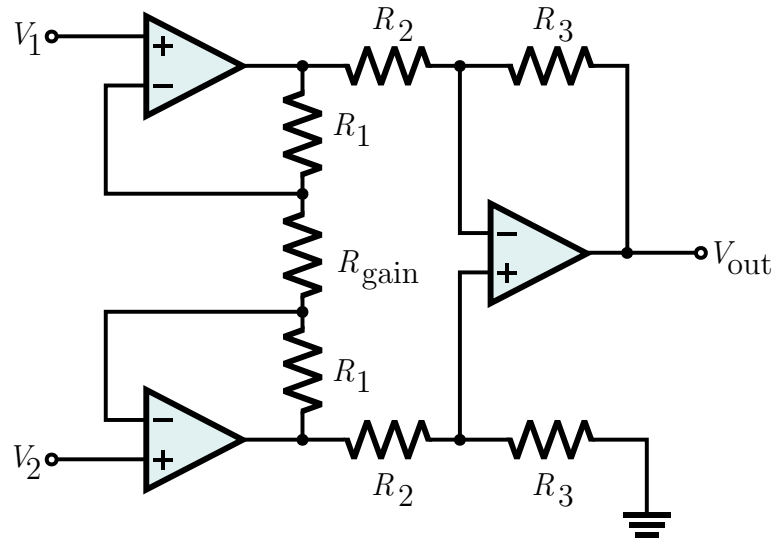


Figure 3.6: Illustration of an instrumentation Amplifier ((WikimediaCommons 2009b))

each second, giving a continuous output. Buck converters are much more efficient compared to linear regulators, which dissipate the voltage drop as heat.

3.3 Microcontroller

This project includes using digital control to stabilize a magnetic levitation platform. For digital control, it was chosen to use a microcontroller. More about the choice of controller in chapter 5 Design. This subsection will therefore give the theoretical framework needed to understand different functions of a microcontroller.

3.3.1 Analog- and digital signals

Analog signals are continuous electrical signals that conveys the data either in the voltage, the current, or the frequency of the signal. Digital signals convey the data through discrete signals. Binary numbers are conveyed through alternating the voltage from the maximum voltage to 0 voltage in discrete time steps. The maximum voltage of a microcontroller is typically either 3.3V or 5V.

3.3.2 PWM-signals

Pulse Width Modulation (PWM) is a technique used to replicate an analog system by transmitting a discrete square wave signal that rapidly changes between transmitting at maximum voltage and sending no voltage. A PWM signal runs on a certain frequency which lasts a period T . The time the PWM signal is "on" in a period T corresponds to the signals duty cycle. The strength of the signal is therefore usually displayed as a % of duty cycle. Figure 3.7 is a simple illustration of 25%, 50% and 75% duty cycle.

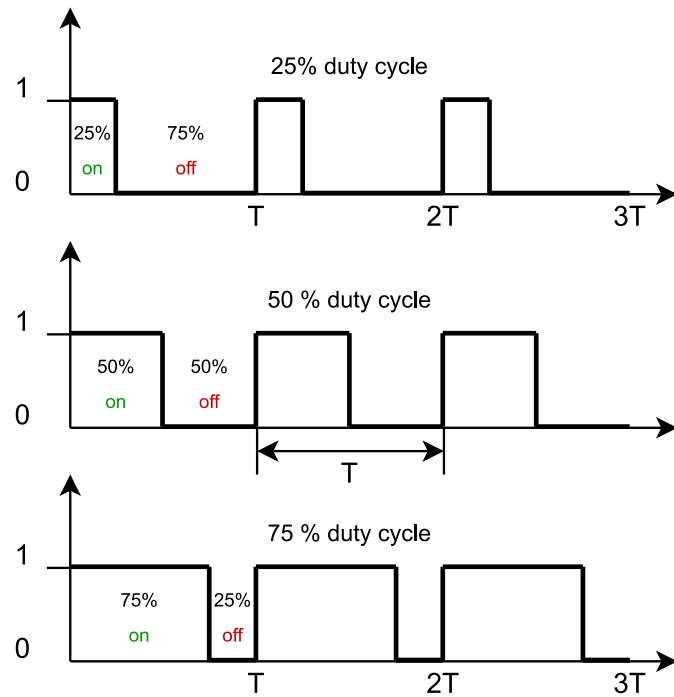


Figure 3.7: Illustration of PWM signals made in diagrams.net

3.3.3 ADC

An Analog to Digital Converter (ADC) is an electric circuit that converts an analog signal to a digital signal. There are many different techniques one may use in an ADC. An example of one is a Successive approximation ADC, which is used in the Teensy 4.0. It uses an Op-Amp as a comparator with the input signal and a reference signal created by a Digital to Analog Converter (DAC) as inputs. The reference signal starts with the value which is equal to a digital signal where the Most Significant Bit (MSB) equals 1, and the rest equals zero. If the input signal has a greater voltage of the reference signal the MSB of the reference signal is locked to 1, otherwise it is set to 0. The reference signal then sets

the next MSB to 1, and another check is done. This continues until all the bits of the reference signal are checked. The reference signal is an approximation of the input signal with an uncertainty of a single bit. The reference signal is then sent out as the output.

3.4 PID-controller

PID-control is one of the most widely used control strategies today, mainly because of its simplicity and efficiency (Knospe 2006). The output of a PID-controller consists of the sum of Proportional, Integral and Derivative terms as shown below.

$$u(t) = u_p(t) + u_i(t) + u_d(t) \quad (3.7)$$

3.4.1 Proportional

The proportional term responds to the current error. The K_p value is often referred to as the proportional gain, and corresponds to how fast the controller responds to a sudden change in error. The proportional term is:

$$u(t) = K_p \cdot e(t) \quad (3.8)$$

3.4.2 Integral

The integral term aims to removes steady state error. This is done by accumulating the error from the proportional term, to increase the correction factor. It is the scale of the integral time, T_i , that states how fast the integral term increases. The integral term is:

$$u_i(t) = K_i \int_0^t e(t) dt \quad (3.9)$$

where

$$K_i = \frac{K}{T_i} \quad (3.10)$$

3.4.3 Derivative

The derivative term minimizes the overshoot by slowing down the correction factor, before the steady state error is zero. The derivative term is:

$$u_d(t) = K_d \cdot \frac{de(t)}{dt} \quad (3.11)$$

where

$$K_d = K \cdot T_d \quad (3.12)$$

The proportional, integral and derivative terms then add up to the PID-equation:

$$u(t) = K_p \cdot e(t) + K_i \int_0^t e(t) dt + K_d \cdot \frac{de(t)}{dt} \quad (3.13)$$

4 Mathematical model and simulation

This section covers the mathematical framework used to model the system and how it was used to find a reasonable magnet configuration. This includes Matlab implementation, modelling of physical components and simulations of the modelled system. Finally, the results from the modelling is discussed, with possible future work and suggested improvements on the methods used in this project.

4.1 System description

A basic illustration of the magnetic levitation platform is shown in figure 4.1. 8 groups of Permanent magnets (coloured grey) are placed in a circle centered on the platform, creating a permanent magnet field. To get a stronger field each group consist of three neodymium magnets stacked on top of each other. 4 Solenoids (coloured red) are placed on a circle inside the permanent magnet circle. The combination of the permanent magnetic field and the controllable magnetic field from the solenoids should in theory make it possible to magnetically levitate a disc magnet (coloured blue) in the air.

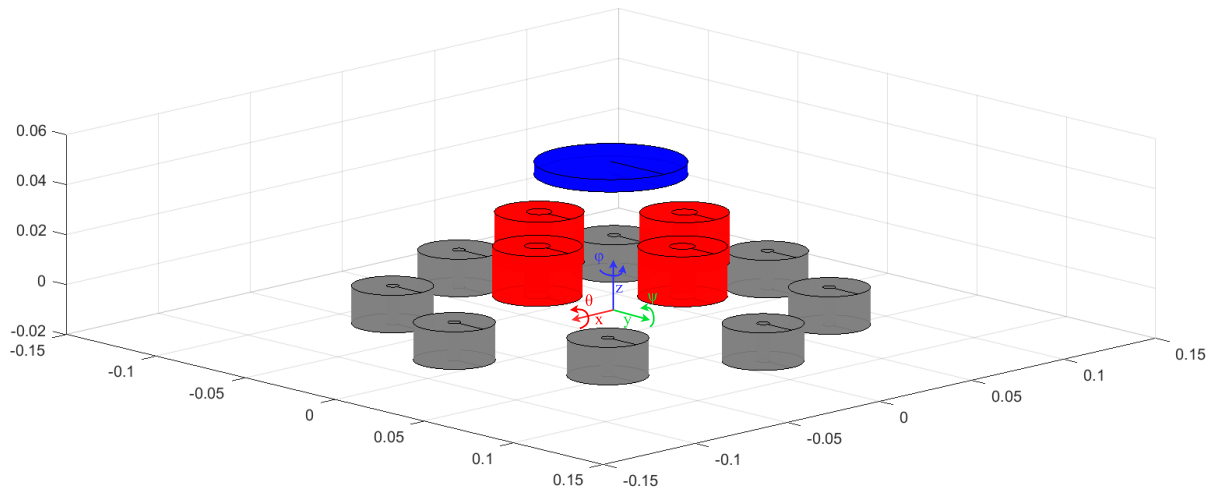


Figure 4.1: System illustration with coordinate frame. The origin is aligned with the top of the permanent magnets.

4.2 Mathematical model

The mathematical model is based on the existing model described in the internal document *Model Description: Magnetic Levitation System* (Doshmanziari, Engmark and Hoang 2021), hereby referred to as the *Model description*. The document models a magnetic levitation platform equivalent to the one used in this project by treating all the magnets involved as solenoids. The solenoids are then modelled as thin wire loops. Using *Biot-Savart's law* and *Laplace's force law* it is possible to estimate the force from the solenoids on the levitating magnet based on the current in the wire loops. To make the approximation possible the loops are discretized into $n = 100$ linear segments.

The position and angle of the levitating magnet in relation to the coordinate frame in figure 4.1 is described by the state vector:

$$\eta = [x_m, y_m, z_m, \psi_m, \theta_m, \phi_m, \dot{x}_m, \dot{y}_m, \dot{z}_m, \dot{\psi}_m, \dot{\theta}_m, \dot{\phi}_m]^T \quad (4.1)$$

Although the model description is made for an equivalent system some adjustments has been made during this project to fit the new system. The permanent magnets were originally modelled as bias current in the solenoids. To get a more accurate representation of the total field generated, the permanent magnets are instead modelled as separate solenoids, but with a set current. This allows for the position of the permanent magnets to be changed in simulations without having to approximate the bias current each time.

4.2.1 Measurements

The model description also assumes full state feedback, which the new system does not have. The measurements are instead the magnetic field in x-, y- and z-direction, as measured by three hall-effect sensors placed in the positions:

$$\begin{aligned} p_x &= \begin{bmatrix} 0 & 0 & 0.004 \end{bmatrix}^T \\ p_y &= \begin{bmatrix} 0 & 0 & 0.004 \end{bmatrix}^T \\ p_z &= \begin{bmatrix} 0 & 0 & 0.009 \end{bmatrix}^T \end{aligned} \quad (4.2)$$

Using Biot-Savarts law with the sensor positions as the points of interest the measurements can be described by the vector function $h(\eta, u)$. The model description presents the following simplification of Biot-Savarts law, as originally described in the paper from (González and Cárdenas 2020):

$$\begin{aligned}\mathbf{B}_\rho(\rho, z) = & \frac{\mu_0 I}{2\pi\sqrt{(\rho' + \rho)^2 + (z - z')^2}} \left\{ \frac{(z - z')}{\rho} \cdot \left[\frac{\rho'^2 + \rho^2 + (z - z')^2}{(\rho - \rho')^2 + (z - z')^2} E(k) - K(k) \right] \mathbf{e}_\rho \right. \\ & \left. - \left[\frac{\rho^2 - \rho'^2 + (z - z')^2}{(\rho - \rho')^2 + (z - z')^2} E(k) - K(k) \right] \mathbf{e}_z \right\}\end{aligned}\quad (4.3)$$

$$k = \frac{4\rho'\rho}{(\rho' + \rho)^2 + (z - z')^2}$$

Where ρ' and z' are the radius and height of the wire loop. $K(k)$ and $E(k)$ are the elliptic integrals of the first and second kind. The limit case of when $\rho \rightarrow 0$ is also presented as:

$$\mathbf{B}_z = \frac{\mu_0 \rho'^2 I}{2 [\rho'^2 + (z - z')^2]^{3/2}} \quad (4.4)$$

In order to calculate the magnetic field in a point using cartesian coordinates, $p = [x, y, z]^T$, the following equations are used.

$$\begin{aligned}\mathbf{B}_x(p) &= \mathbf{B}_\rho(\rho, z) \cos \phi \\ \mathbf{B}_y(p) &= \mathbf{B}_\rho(\rho, z) \sin \phi \\ \mathbf{B}_z(p) &= \mathbf{B}_z(\rho, z)\end{aligned}\quad (4.5)$$

Expanding the equations from the model description to include the permanent magnets we get:

$$h(\eta, u) = \vec{\mathbf{B}} = \sum_{i=1}^m \begin{bmatrix} B_x(p_x - p_s^i) \\ B_y(p_y - p_s^i) \\ B_z(p_z - p_s^i) \end{bmatrix} + \sum_{j=1}^n \begin{bmatrix} B_x(p_x - p_m^j) \\ B_y(p_y - p_m^j) \\ B_z(p_z - p_m^j) \end{bmatrix} \quad (4.6)$$

for a system with m solenoids and n permanent magnets, where p_s^i is the center of the i 'th solenoid and p_m^j is the center of the j 'th permanent magnet. p_x , p_y and p_z is the positions of the three hall effect sensors.

The system can then be represented by the equations:

$$\begin{aligned}\dot{\eta} &= A\eta + B\phi(\eta, u) \\ y &= h(\eta, u)\end{aligned}\quad (4.7)$$

Where, like in the model description:

$$\begin{aligned} A &= \begin{bmatrix} O_{6x6} & I_6 \\ O_{6x6} & O_{6x6} \end{bmatrix} \\ B &= \begin{bmatrix} O_{6x6} \\ I_6 \end{bmatrix} \end{aligned} \quad (4.8)$$

and

$$\phi(\eta, u) = \begin{bmatrix} mI_3 & O_{3x3} \\ O_{3x3} & \mathcal{I} \end{bmatrix}^{-1} \begin{bmatrix} F_b(\eta, u) \\ \tau_b(\eta, u) \end{bmatrix} - \begin{bmatrix} O_{8x1} \\ g \\ O_{3x1} \end{bmatrix} \quad (4.9)$$

4.2.2 Equilibrium

Analysing if and where the system is in equilibrium is useful when deciding on an operating point for the controller. The system is in equilibrium if:

$$\dot{\eta} = A\eta + B\phi(\eta, u) = \mathbf{0} \quad (4.10)$$

Which for an autonomous system ($u = \mathbf{0}$) becomes:

$$\dot{\eta} = \begin{bmatrix} \dot{x}_m \\ \dot{y}_m \\ \dot{z}_m \\ \dot{\psi}_m \\ \dot{\theta}_m \\ \dot{\phi}_m \\ F_x/m \\ F_y/m \\ F_z/m - g \\ \tau_\psi/\mathcal{I} \\ \tau_\theta/\mathcal{I} \\ \tau_\phi/\mathcal{I} \end{bmatrix} = \mathbf{0} \quad (4.11)$$

Using equation 4.7. Due to symmetries in the permanent magnetic field, if:

$$x_m = y_m = \psi_m = \theta_m = \phi_m = 0 \quad (4.12)$$

then:

$$F_x = F_y = \tau_\psi = \tau_\theta = \tau_\phi = 0 \quad (4.13)$$

By also assuming the following stationary conditions:

$$\dot{x}_m = \dot{y}_m = \dot{z}_m = \dot{\psi}_m = \dot{\theta}_m = \dot{\phi}_m = 0 \quad (4.14)$$

the only non-zero element in 4.11 is $F_z/m - g$. Given the states in equation 4.12, equation 4.14 and $u = \mathbf{0}$, F_z only varies with z_m . This means that if there exist an $z_{m,eq}$ such that $F_z/m - g = 0$, then there exists an unstable equilibrium in (η_{eq}, u_{eq}) :

$$\left. \begin{aligned} \eta_{eq} &= \left[0 \ 0 \ z_{m,eq} \ 0 \ 0 \ 0 \ 0 \ 0 \ 0 \ 0 \right]^T \\ u_{eq} &= \left[0 \ 0 \ 0 \ 0 \right]^T \end{aligned} \right\} \Rightarrow \dot{\eta} = \mathbf{0} \quad (4.15)$$

Finding $z_{m,eq}$ for the system in this project was done numerically in Matlab, as explained further in section 4.3.3.

4.3 Matlab implementation

The mathematical framework from the model description has been implemented as a Matlab model to simulate the system. A GitHub repository¹ has been made, containing the original code written by the authors of the model description (Doshmanziari, Engmark and Hoang 2021) as well as the code written specifically for this project. The following subsections will go through how the code works and how it has been applied.

4.3.1 Class definition

The class *maglevSystem* has methods for computing the magnetic field of the solenoids and permanent magnets, the force and torque on the levitating magnet and the state derivative $\dot{\eta}$. An object of this class can be used to simulate the trajectory of the levitating magnet given the current in each solenoid. Code listing 4.1 shows how an object from the *maglevSystem* class might be created. The *params* variable is a struct containing all the relevant specifications of the system. A detailed list of all the parameters in *params* can be found in appendix F.

¹https://github.com/martinbronstad/Bachelor_Thesis_E2207

```

1 approximationType = 1;           % Accurate approximation
2 load('params.mat');            % Loading system parameters
3
4 %% Initializing the system
5 x0 = zeros(12,1);
6 x0(3) = 0.0475;                % Initial z-coordinate
7 sys = maglevSystem(x0, params, approximationType);

```

Listing 4.1: Creating a system object from the *maglevSystem* class

4.3.2 Accurate and fast simulations

The *maglevSystem*-class has two main modes of approximating the magnetic field: fast and accurate. The fast mode models each solenoid as one discretized wire loop centered in the solenoid's mass as shown in figure 4.2a. The computed force and torque are then scaled up by the number of windings in the solenoid, where $windings = nr \cdot nh$. When using the accurate mode each winding is treated as separate wire loops distributed across the volume of the solenoid, with nr concentric loops in width and nh loops in height as shown in figure 4.2b. This is a more time consuming way to simulate the system as the magnetic field has to be computed separately for each winding, but it also gives a more accurate representation of the actual system given that the number of windings is set up correctly.

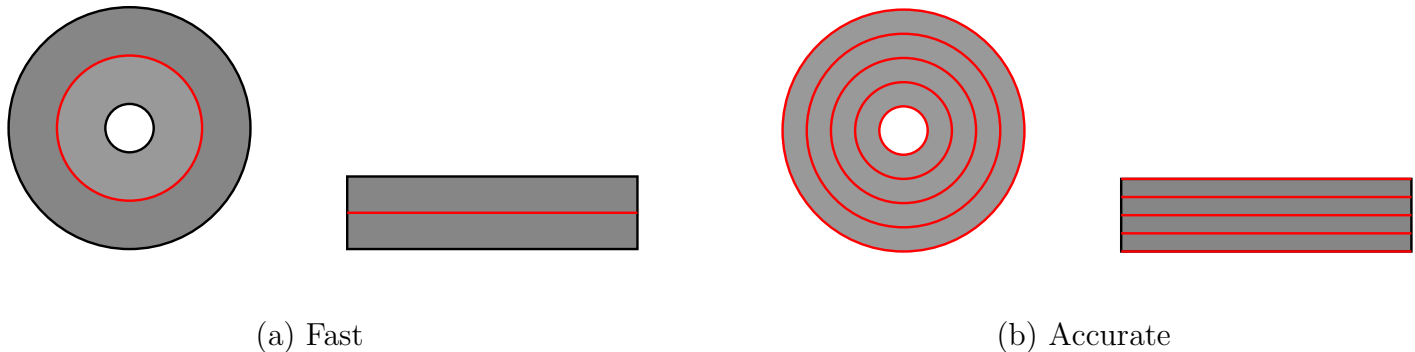


Figure 4.2: Top and side view of a solenoid modelled with the two different methods. This example has $nr = 5$ and $nh = 5$.

4.3.3 Z-graph

As mentioned in section 4.2.2, the levitating magnet will be in equilibrium at a height $z_{m,eq}$ such that:

$$\frac{F_z(z_m)}{m} - g = 0 \quad (4.16)$$

Using the *maglevSystem*-class to graph $F_z/m - g$ while varying z_m produces a plot like the one shown in figure 4.3. $z_{m,eq}$ is found numerically in Matlab by analysing where the graph crosses zero. The graph in figure 4.3 has two equilibria, at $z_m = 0.002$ and $z_m = 0.047$. $z_m = 0.002$ is unstable in the z-direction, perturbing the levitating magnet at this height will make it diverge. $z_m = 0.047$ is the opposite, when moving along the z-axis away from this equilibrium the permanent magnet field will push the magnet back towards $z_m = 0.047$. It is therefore logical to choose the latter as the operating point of the system.

In addition to finding the equilibrium, a z-graph is useful for characterizing different magnet configurations, for example by analysing how much force is needed from the solenoids to move the levitating magnet vertically. This technique is used in section 4.5.1.

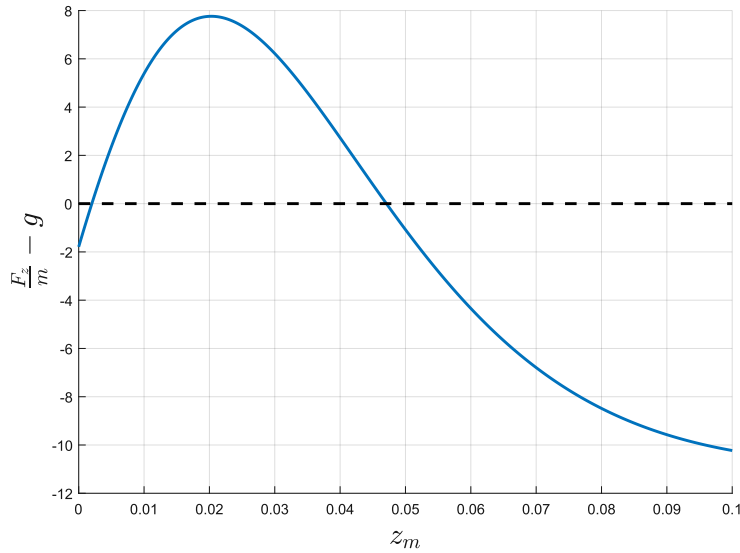


Figure 4.3: Example of a z-graph. The z-position of the levitating magnet z_m is on the x-axis.

4.4 Modelling the physical components

In order to make the Matlab model represent the physical system in a good way it was necessary to model the physical components. This was done in the most part by measuring the physical dimensions of the permanent magnets, the levitating magnet and the solenoids. In addition to this the strength of the permanent and levitating magnets had to be estimated. As mentioned in section 4.2 the permanent

and levitating magnets were modelled as solenoids with a set current. This meant finding a current such that the field strength of the modelled solenoids matched the field strength of the real magnets. A detailed list of all the parameters found in this section is attached as appendix F.

4.4.1 Neodymium magnets

As the permanent magnets were to be grouped in stacks of three, it was natural to model one stack as one solenoid. Finding the equivalent current was done by applying the equilibrium conditions from equation 4.15 on a simplified system as shown in figure 4.4. The system consisted of two stacks of three neodymium magnets where one was fastened to a surface, acting as the permanent magnets, while the other stack was suspended above, acting as the levitating magnet. By measuring $z_{m,eq}$ the only unknown was the current needed to create the force F_z . By simulating an equivalent system in Matlab it was possible to find the current numerically. Using the parameters in table 4.1 $z_{m,eq}$ was measured to be 0.09m, corresponding to an equivalent solenoid current of -43.22 .

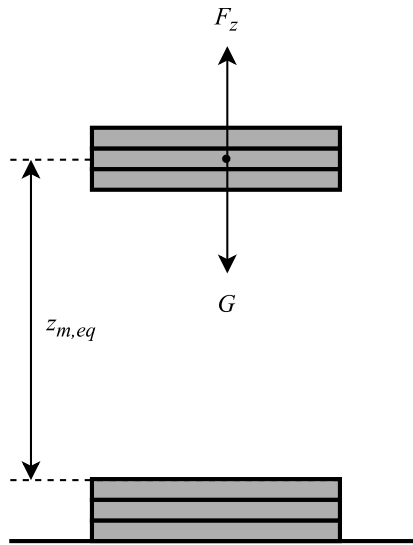


Figure 4.4: Measuring levitating height between two stacks of three neodymium magnets

Dimension	Variable	Value	Unit
Inner radius	ri	0.0025	m
Outer radius	ro	0.016	m
Height	h	0.015	m
Mass	m	0.072	kg
Number of rings in radius	nr	20	
Number of rings in height	nh	25	
Levitating height	$z_{m,eq}$	0.09	m
Equivalent current	I	-43.22	

Table 4.1: Specifications for a stack of three neodymium magnets

4.4.2 Levitating magnet

The levitating magnet was modelled using the same technique as with the permanent magnets. The levitating height had to be measured between a stack of three neodymium magnets and the levitating magnet as there is only one levitating magnet. Since the equivalent current of a stack of three neodymium magnets was known, this could be used to find the current for the levitating magnet in Matlab. $z_{m,eq}$ was measured to be 0.065m , corresponding to an equivalent solenoid current of -9.1 .

Dimension	Variable	Value	Unit
Inner radius	ri	0.00	m
Outer radius	ro	0.03	m
Height	h	0.005	m
Mass	m	0.117	kg
Number of rings in radius	nr	20	
Number of rings in height	nh	25	
Levitating height	$z_{m,eq}$	0.065	m
Equivalent current	I	-9.10	

Table 4.2: Specifications for the levitating magnet

4.4.3 Solenoids

The physical dimensions of the solenoids were measured as shown in table 4.3. As described in section 5.2.3, the maximum current through each solenoid was found to be 0.5A.

Dimension	Variable	Value	Unit
Inner radius	ri	0.005	m
Outer radius	ro	0.0175	m
Height	h	0.02	m
Number of rings in radius	nr	20	
Number of rings in height	nh	50	
Offset along z-axis	z_s	0.023	m

Table 4.3: Specifications for the solenoids

4.5 Finding a reasonable configuration

4.5.1 Permanent magnets

As mentioned in section 4.1, the permanent magnets would be placed in stacks of three on a circle around the center of the platform. The radius of said circle would impact both the stability of the system as well as the flexibility of the levitating magnet, i.e. how much force was needed to move the magnet away from equilibrium.

Figure 4.5 shows the z-graph for four different permanent magnet setups with increasing radius. Lower radius means a more rigid equilibrium as the force from the permanent magnets are stronger with small deviations. Higher radius yields a more flexible system, requiring less force from the solenoids to manipulate the height of the levitating magnet. However, too high radius means the system won't have an equilibrium. As a starting point a radius of $R = 0.085m$ was chosen, as this setup in theory allowed for some movement in the z-direction while not being close to instability. In addition this configuration made room for bigger spacing between the solenoids which we assumed would make the control even more flexible. This setup meant an equilibrium at $z_{m,eq} = 0.0471m$, which was used as the operating point of the system.

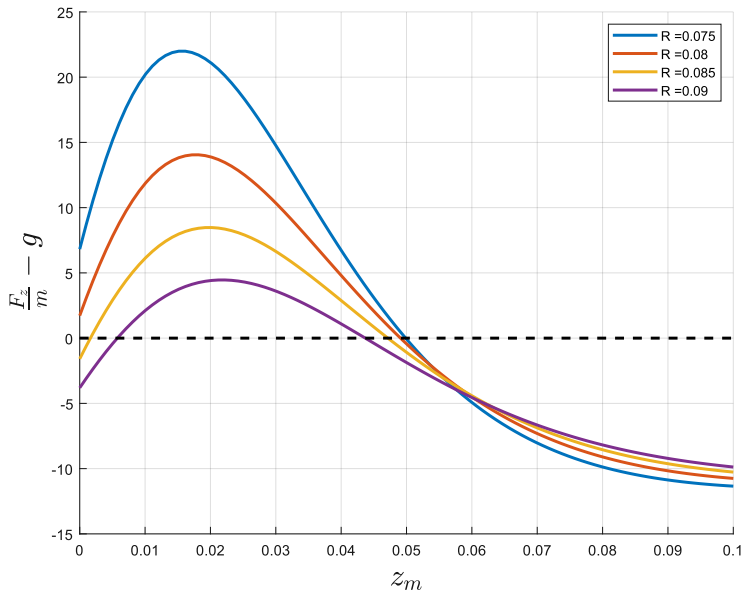


Figure 4.5: Z-graph for four different permanent magnet configurations

4.5.2 Solenoids

The four solenoids would also be placed on a circle around the center of the platform. The main concern regarding the solenoid positions was how strong the force from the solenoids on the levitating magnet would be. Using the same idea as in section 4.3.3 the force in the x- and y-direction (F_x and F_y) was plotted while moving the magnet along the x- and y-axis respectively, with $z_m = z_{m,eq}$. Running such a test with maximum current in the solenoids gave an idea of how much impact the controller could have on the position of the levitating magnet in different configurations. Figure 4.6 shows the difference in F_x between zero current and maximum current in the solenoids on the x-axis. The radius at which the solenoids are placed is $R = 0.04m$. Note that the two solenoids have opposite polarity, which in this case means that they are pulling the levitating magnet in negative x-direction. Plotting a similar graph with $u = \begin{bmatrix} 0.0 & -0.5 & 0.0 & 0.5 \end{bmatrix}^T$ would produce an inverse graph. Using figure 4.6 as a reference, the solenoids should in theory be able to correct a deviation from the origin along the x- and y-axis of up to $\approx 0.04m$, which was assumed to be more than enough for a system of this size.

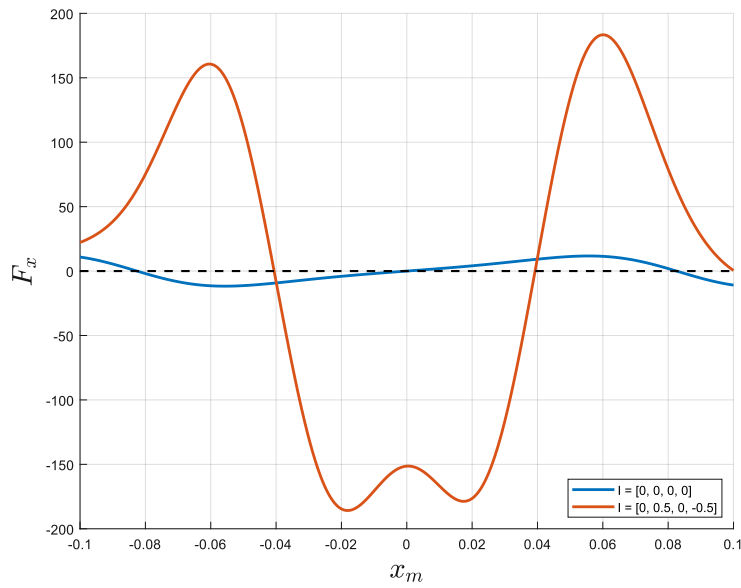


Figure 4.6: Force in x-direction with no current vs max current in solenoids

In addition to the radius of the solenoid positions, the height at which they were placed (z_s) would also impact the control. The layered design of the platform, as described in section 5, made it natural to test a configuration with the solenoids placed one layer above the permanent magnets, which corresponds to $z_s = 0.023$. Figure 4.7 shows the difference in F_x between the two solenoid configurations with $u = \begin{bmatrix} 0.0 & 0.5 & 0.0 & -0.5 \end{bmatrix}^T$. Moving the solenoids up one layer had a significant impact on the strength transferred to the levitating magnet, and was therefore chosen as the preferred configuration.

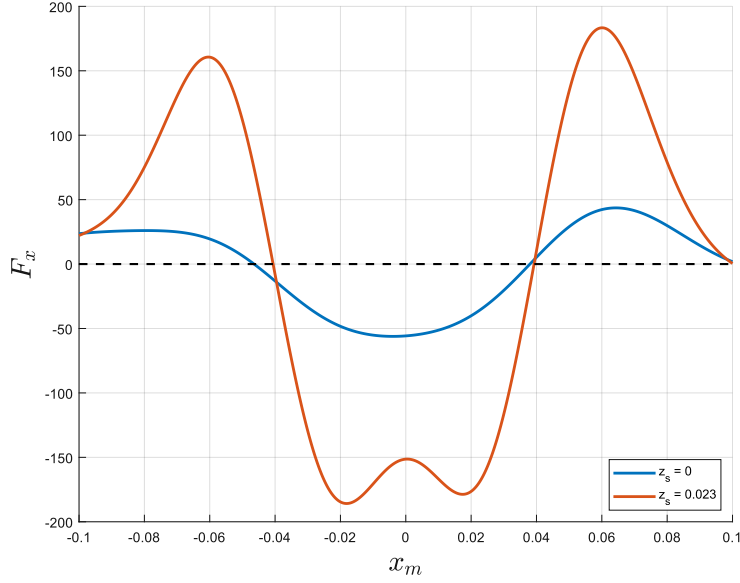


Figure 4.7: Force in x-direction with solenoids placed at $z_s = 0$ vs $z_s = 0.023$

4.6 Linear analysis

4.6.1 Linearization

Linearization of the system around the operating point (η_{eq}, u_{eq}) (see equation 4.15) was done to make the system easier to analyse and eventually implement a controller on. The linearized system can be expressed as:

$$\begin{aligned} \dot{\eta} &= A\eta + Bu \\ y &= C\eta \end{aligned} \tag{4.17}$$

The matrices A , B and C were found by taking the partial derivatives of the existing system with respect to η and u (Andresen, Balchen and Foss 2016):

$$\dot{\eta} = f(\eta, u) \tag{4.18}$$

$$A = \left[\frac{\partial f}{\partial \eta_1} \Big|_{(\eta_{eq}, u_{eq})} \quad \frac{\partial f}{\partial \eta_2} \Big|_{(\eta_{eq}, u_{eq})} \quad \dots \quad \frac{\partial f}{\partial \eta_{12}} \Big|_{(\eta_{eq}, u_{eq})} \right] \tag{4.19}$$

$$B = \left[\frac{\partial f}{\partial u_1} \Big|_{(\eta_{eq}, u_{eq})} \quad \frac{\partial f}{\partial u_2} \Big|_{(\eta_{eq}, u_{eq})} \quad \dots \quad \frac{\partial f}{\partial u_4} \Big|_{(\eta_{eq}, u_{eq})} \right] \tag{4.20}$$

$$C = \begin{bmatrix} \frac{\partial h}{\partial \eta_1} \Big|_{(\eta_{eq}, u_{eq})} & \frac{\partial h}{\partial \eta_2} \Big|_{(\eta_{eq}, u_{eq})} & \cdots & \frac{\partial h}{\partial \eta_{12}} \Big|_{(\eta_{eq}, u_{eq})} \end{bmatrix} \quad (4.21)$$

The partial derivatives could not be solved analytically and had to be approximated using the following finite difference approximation:

$$\frac{\partial f(\eta, u)}{\partial \eta} \approx \frac{f(\eta + \Delta, u) - f(\eta - \Delta, u)}{2\Delta} \quad (4.22)$$

Where Δ is the step size.

```

1 %% Linearization
2 delta = 1e-4;
3 A = zeros(12,12);
4 for i = 1:12
5     A(:,i) = ...
    (sys.f(xLp+(i==1:12)']*delta,uLp)-sys.f(xLp-(i==1:12)']*delta,uLp)) / (2*delta);
6 end
7
8 B = zeros(12,params.solenoids.N);
9 for i = 1:4
10    B(:,i) = ...
    (sys.f(xLp,uLp+(i==1:4)']*delta)-sys.f(xLp,uLp-(i==1:4)']*delta)) / (2*delta);
11 end
12
13 C = zeros(3*length(params.sensor.x),12);
14 for i = 1:12
15    C(:,i) = (sys.h(xLp+(i==1:12)']*delta, uLp)-sys.h(xLp-(i==1:12)']*delta, ...
    uLp)) / (2*delta);
16 end

```

Listing 4.2: Linearization in Matlab

4.6.2 Transfer function matrix

Using the linearized model from section 4.6.1, the transfer function matrix $G(s)$ can be found:

$$G(s) = C[sI - A]^{-1}B = \begin{bmatrix} g_{11}(s) & g_{12}(s) & g_{13}(s) \\ g_{21}(s) & g_{22}(s) & g_{23}(s) \\ g_{31}(s) & g_{32}(s) & g_{33}(s) \\ g_{41}(s) & g_{42}(s) & g_{43}(s) \end{bmatrix} \quad (4.23)$$

With $G(s)$ being a 4x3 matrix, one row per input and one column per output. The code in listing 4.3 was used to generate the transfer function matrix in Matlab.

```
1 ssModel = ss(A,B,C,D); % State space model
2 tfModel = tf(ssModel); % Creating a transfer function matrix
3 G = [tfModel(1,:); tfModel(5,:); tfModel(9,:)];
```

Listing 4.3: Finding the transfer function matrix in Matlab

As explained in further detail in section 6, the controller was set up with three parallel PID-controllers actuating the four inputs. Figure 6.1 shows the control structure. To model the output algorithm implemented on the microcontroller we needed to find $H_c(s)$ such that:

$$H_c(s) \cdot \mathbf{u} = H_c(s) \begin{bmatrix} u_x & u_y & u_z \end{bmatrix}^T = \begin{bmatrix} u_y + u_z \\ u_x + u_z \\ -u_y + u_z \\ -u_x + u_z \end{bmatrix} \quad (4.24)$$

Which corresponds to this matrix:

$$H_c(s) = \begin{bmatrix} 0 & 1 & 1 \\ 1 & 0 & 1 \\ 0 & -1 & 1 \\ 1 & 0 & 1 \end{bmatrix} \quad (4.25)$$

$$H(s) = H_c \cdot G(s) = \begin{bmatrix} h_{11}(s) & h_{12}(s) & h_{13}(s) \\ h_{21}(s) & h_{22}(s) & h_{23}(s) \\ h_{31}(s) & h_{32}(s) & h_{33}(s) \end{bmatrix} \quad (4.26)$$

Both $H(s)$ and the state space matrices can be found in the GitHub repository as *sysMatrices.mat*. The state space matrices is also listed in appendix G. The high order and the pole-zero-placement of the transfer functions made it difficult to use any familiar techniques to find controller parameters.

4.6.3 Condition number and RGA

The linearized system from section 4.6.1 analysed using singular value analysis (Skogestad and Postlethwaite 2007) and Bristol's Relative Gain Array Method (Bristol 1966; Seborg et al. 2016). This was done to determine the level of interaction between loops and to verify that the input-output pairings chosen in section 6.1 were reasonable.

$$H_0 = \lim_{s \rightarrow 0} sH(s) = \begin{bmatrix} -4.136 & 0.0006 & -0.0113 \\ 0.0317 & -4.122 & 0.0108 \\ -0.0203 & 0.0146 & -2.8548 \end{bmatrix} \quad (4.27)$$

The *condition number* is given by:

$$\gamma(H_0) = \frac{\bar{\sigma}(H_0)}{\underline{\sigma}(H_0)} \quad (4.28)$$

Where $\bar{\sigma}(H_0)$ and $\underline{\sigma}(H_0)$ are the maximum and minimum singular values of H_0 respectively. A large condition number, Skogestad suggests larger than 10, indicates that the system might be hard to control. On the contrary, a small condition number indicates that the system is insensitive to multivariable disturbances. Using the Matlab command *cond()* returns $\gamma(H_0) = 1.45$. Based on this, the system in its current configuration is of the latter type.

The *Relative Gain Array*, Λ , is traditionally used as an interaction measure between the loops of a multivariable system and as a tool to find the best input-output pairings. The RGA is given by:

$$\Lambda = H_0 \otimes (H_0^{-1})^T = \begin{bmatrix} 1.00 & -2,06 \cdot 10^{-8} & -1,08 \cdot 10^{-5} \\ -5.89 \cdot 10^{-5} & 1.00 & -9.79 \cdot 10^{-6} \\ -3.46 \cdot 10^{-5} & -1.81 \cdot 10^{-5} & 1.00 \end{bmatrix} \quad (4.29)$$

Where each row corresponds to an output and each column corresponds to an input. Ideally one would want to pair the inputs and outputs where the relative gain is close to one. In this case it is trivial to see that pairing u_x with y_x , u_y with y_y and u_z with y_z is close to optimal.

4.6.4 PID implementation

The same incremental PID algorithm implemented on the microcontroller was also implemented in Matlab. This allowed us to simulate the nonlinear system with PID control using Matlab's *ode45* solver. The controller is implemented in the script *PIDsim.m*. See section 6.2.2 for the specifics on the controller algorithm.

4.7 Discussion

Analysing and simulating the system using the mathematical framework described in this section has been a big part of the project. The fact that the mathematical model is fairly advanced means there many possible sources of error. This section will discuss the methods used during the modelling, choice of configuration and mathematical analysis, as well as suggest improvements and expansion for the future.

4.7.1 Modelling the components

A possible source of error in the modelling is the choice of method when finding equivalent currents for the levitating magnet and permanent magnets. The method should in theory produce a result that make the model accurately represent the actual system, but reproducing the conditions presented in equation 4.15 with accuracy is difficult with real components. Ideally the results should be systematically verified by making a test setup where the magnetic field produced by the magnets is measured using hall-effect sensors.

4.7.2 Choice of configuration

The permanent magnet and solenoid configuration were mostly chosen based on the analysis done on the force plots shown in section 4.5.1 and 4.5.2. With more time the shape of the permanent magnet field could be analyzed and compared with the the analog system as shown in figure 6.10. Using this an extra metric of stability could possibly be helpful in choosing a setup.

4.7.3 Fast and accurate simulations

The difference between the fast and accurate simulations was bigger than expected at the start of the project due to a scaling issue between the two modes. This meant that the same equivalent currents

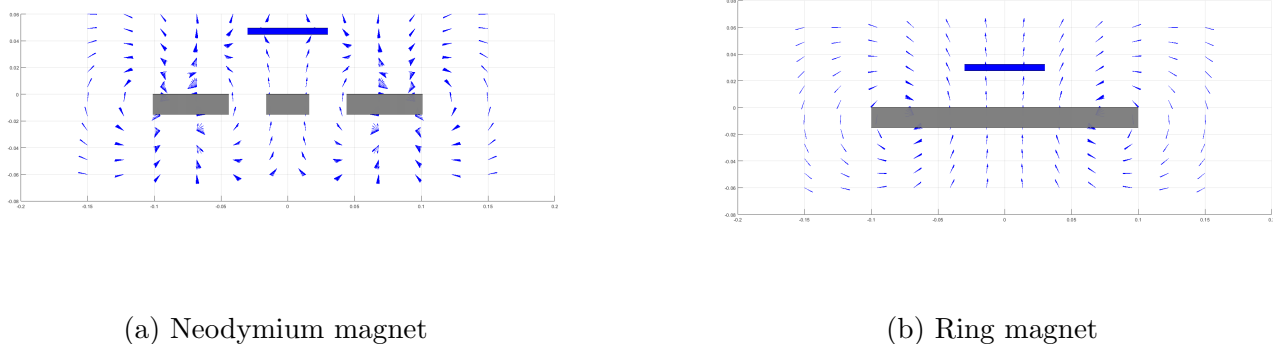


Figure 4.8: Comparison of simulated permanent magnetic fields

in the same solenoids gave different results depending on the simulation mode used. Slightly increasing the radius of the single wire loop used in the fast simulations (from 0.015m to 0.020m for the levitating magnet) was tried as a workaround. This gave the desired results for this specific system. However, this is not a permanent solution to the problem, as changing the system parameters most likely would require the wire loop radius to be changed again. For the future it is recommended to look further into this issue and find a better connection between the two modes.

4.7.4 Verification of the model

Although the model seems to represent the physical system in a good way, there has been no systematic testing to confirm that this is the case. With more time and a stable system model verification would have been prioritized, as a good model is crucial to further development of the platform.

4.7.5 Controller parameters

As mentioned in section 4.6.2, the transfer functions of the linearized system was difficult to work with due to the nature of the system. Several different methods was tried to approximate the system without satisfying results. The resulting transfer function usually contained poles and zeros on the imaginary axis or in the right half plane, making it difficult to use methods like SIMC (Grimholt and Skogestad 2018) to find controller parameters. Using a different control structure could improve upon this problem, for example by using cascade control. The *inner feedback loop* could then stabilize the right half plane poles while an outer loop controller gives the system the desired characteristics.

5 Design

The design was split between two different sections, the physical design and the electrical design. This chapter will include and explain the different choices and methods used during the design phase.

5.1 Physical system

To design the physical system an overview of the requirements were made. A chassis would need to house all the electronics, be modular to allow changes in configurations, protect against the levitating magnet and to meet the required placement specifications for the permanent magnets and the solenoids.

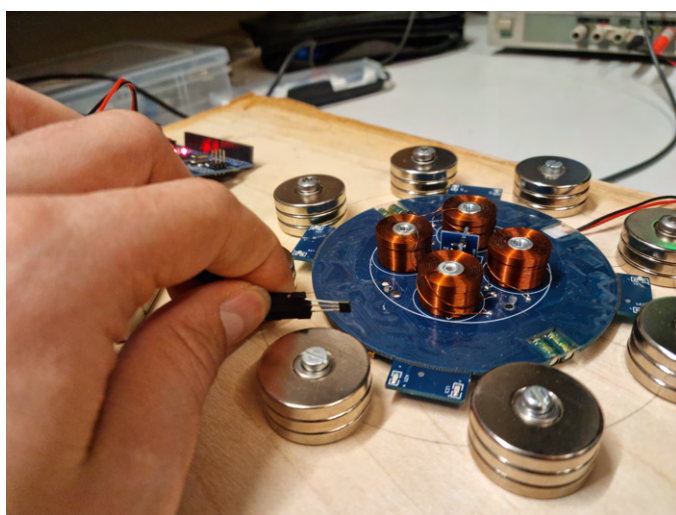
5.1.1 Testing

During the planning phase of the project, a configuration regarding the placement of both the permanent magnets and the solenoids had to be chosen. The configuration was chosen alongside the simulations, shown in section 4.5.2. During this phase the modelling in the simulations were based on physical tests of the permanent magnets and solenoids. It was then tested different configurations of permanent magnets, with the analog system as shown in figure 5.1. During the testing it was figured out that due to the strength of the permanent magnetic field, the solenoids had to be raised to a higher level. As shown in figure 5.1b the levitating magnet was stable when the analog solenoids were raised high enough.

Regarding the material of the prototyping plates, the wooden prototype bases proved to be difficult to make accurately. They were clunky and pieces of wood would often splinter off. This in turn resulted in inaccurate mounting positions, which could affect both the sensor measurements and the magnetic fields. A more robust material was needed. Materials considered were various metals, 3D-printed plastics and plexi-glass. Plexi-glass was chosen as it is neither magnetic or heavy, yet it is durable and strong.

As mentioned in section 2.1 there were two sets of solenoids and electromagnets bought. The solenoids are larger than the electromagnets, with 1000 windings. The electromagnets are smaller with 500 windings, but has an iron core which can be magnetized. The current limit of these were tested with a variable power supply. At 12V the solenoids generated 0.7A of current. Running the solenoids with a continuous current of 0.7A would make the solenoids too hot. However, due to the fact that the solenoids would not get a continuous current of 0.7amp during normal operational conditions, this was still considered acceptable as an upper current limit. The tests were also run on the smaller electromagnets as shown in figure 5.2. However, as they have a lower resistance, they would get extremely hot at 12 V. They were

therefore capped at 4.6 V, at which they would draw approximately 0.7A.



(a) Wood test base



(b) Testing the analog system

Figure 5.1: Testing magnet distances with the analog system

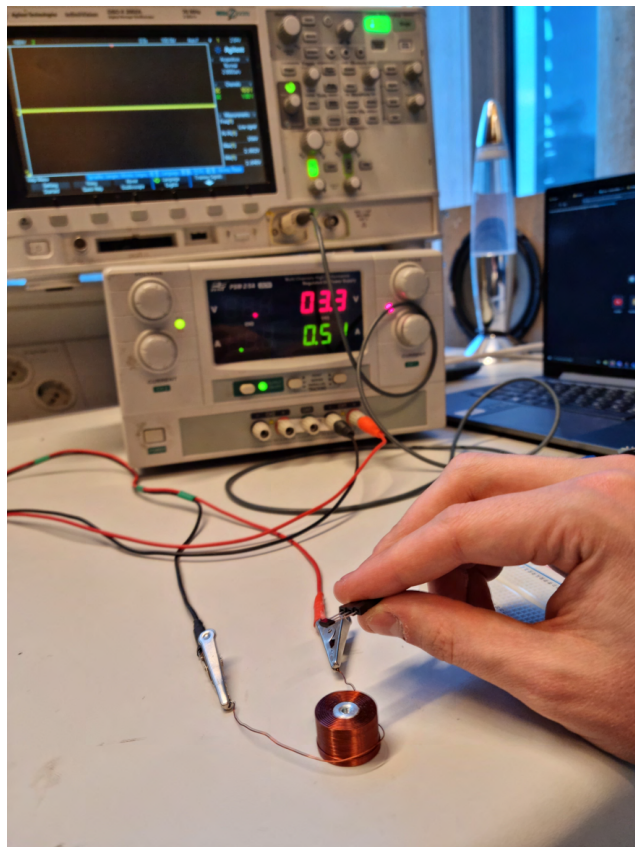
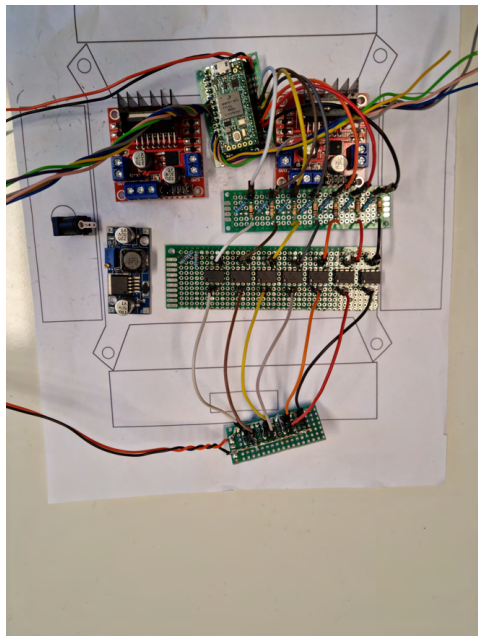


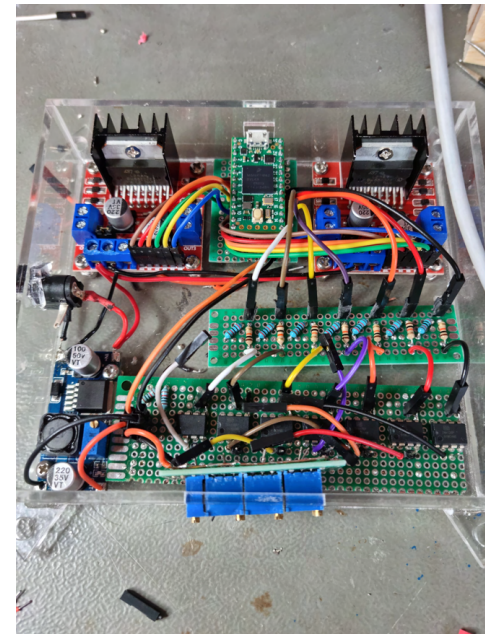
Figure 5.2: Testing the maximum current

5.1.2 System housing

Originally the system was designed to consist of three different layers. The lower layer was to house the electronics, the middle layer to house both the solenoids and permanent magnets and the top layer would work as a protective layer safeguarding the system from the falls of the levitating magnet. During the testing phase described in section 5.1.1, it was discovered that the magnetic fields from the solenoids were too weak to control the levitating magnet from the same height as the permanent magnets. As the system was designed to be modular this wasn't a problem, and another layer was added to mount only the solenoids. This layer was raised above the permanent magnets by 18mm. To determine the required size of the housing the electrical components, the electronics were measured and placed on a prototype paper print as shown in figure 5.3a. This resulted in the housing shown in figure 5.3b.



(a) Housing size estimation



(b) Inserted electrical circuit

Figure 5.3: Electrical housing

The different plexi-glass parts with measurements can be seen in the the plexi-glass schematic in appendix A. This all put together can be seen in figure 5.4. It is shown from the side, and includes measurements of height and width of the different layers.



Figure 5.4: Measurements height

5.1.3 Laser cutting

To reduce errors in both the sensor measurements and the magnetic fields, accuracy was weighted heavily in the design phase. As the wooden test bases made during the planning phase did not meet the wanted requirements, it was decided to make the chassis out of 3mm thick plexi-glass which was designed in Inkscape. Laser cutting has a high accuracy. This would reduce unwanted movement from the fastened components, which could compromise the control. However, the laser cutter only accepted dxf files, and the format used in Inkscape was SVG. The files had to be converted and the conversion resulted in inaccurate scaling of different objects. Most noticeably the diameter of the m6 mounting holes for the solenoids were off by 0.5mm. As the mounting holes were designed to be tight to reduce movement of components, the difference made it impossible to use the planned bolts. The dxf file had to be manually adjusted in the laser cutting software RD-Works and new plexi-glass plates had to be cut. After the laser cutting all the plexi-glass parts were ready to be used, except for the electrical housing. The electrical housing consisted of multiple parts, and had to be glued together by clear epoxy. The mounting holes for the electronics were also drilled manually.

5.1.4 Mounting of sensors

To make the sensors changeable, a "sensor-board" was made. The sensor-board was made of cutouts from protoboards that was glued together by epoxy. The cutouts were used to form a 90° angle where

the sensors would be fastened with epoxy. The base of the protoboard has four mounting screws to fasten the board to the different solenoid layers. This sensor board is seen in figure 5.5.



Figure 5.5: Hall effect sensors epoxied on the sensor-board

5.2 Electronics

As the system was to be modular, the electrical circuit was split into different removable boards. The different boards are connected to each other with wires using pinheaders or jst-connectors. The complete electrical schematic can be seen in appendix D.

5.2.1 Power input

A female DC barrel jack was used as the power input connector due to it giving the user the ability to easily disconnect the power from the system at any moment during operation. From the barrel jack 12V would be directly wired to the motor drivers. However, the rest of the circuit needed 5V. To lower the voltage a buck converter was installed. From the testing in section 5.1.1, it was decided that the upper current limit of the solenoids would be 0.7 Amp. Therefore after calculating the maximum power drain of the system it was decided to use a 12 V, 3A DC power supply. The 3A power supply would be enough to power all the solenoids at the decided upper current limit, while still having enough power for the remaining components.

5.2.2 Microcontroller

As the system has a small area in which the levitating magnet can be stabilized, a fast controller is needed to register and control the small changes in the system. A Raspberry PI was considered, but as the system was designed to be smaller, a microcontroller was preferable. It was decided to use the

Teensy 4.0. It is one of the fastest microcontrollers on the market today, with a clock speed of 600 MHz (Semiconductors 2019). It was resonated that it would be more than fast enough for PID control, when similar working builds used microcontrollers running at 20 MHz (see Funilab 2018).

When transferring data to the Teensy from a computer, a USB cable is used. When connected, the Teensy also receives power from the USB. However, if the Teensy is connected to an external power source as well, it is possible for the excess current to damage the connected computers USB port. The Teensy natively comes with a scrapable connector pad, that if cut, separates the USB and external power circuits. If cut, the Teensy will be unable to be powered by USB and will require an external power source to function. More info about this can be found in appendix E

5.2.3 Motor drivers

To control the direction and power of the solenoids there was added a motor driver to the circuit. The L298N (Sparkfun 2000) was chosen due to it being available in the local area. The group also had experience working with it, and it was within budget. It functions by first receiving two inputs per solenoid to determine the direction of the current, and one PWM input per solenoid to determine the voltage. One downside to the L298N was that they have a considerable voltage drop from the input voltage to the output voltage. However, this was taken into consideration beforehand, and it was expected to have a maximum output voltage at 10.3 V. This would make the new maximum current going through the solenoids 0.5 A.

5.2.4 Sensors

To determine the state of the system there is a need for a sensor to send data to the controller. There are many possible sensors which would be able to determine the position of the levitating magnet, e.g. a motion sensor based on either sound or laser. In this system it was decided to use Hall effect sensors. Hall effect sensors do not directly measure the position of the magnet, but rather the magnetic field. This can be used to determine the position of the magnet, by observing the change of the magnetic field caused by the positioning of the levitating magnet. The reason for using hall effect sensors was that they were inexpensive, small, require no extensive setup, and they were available for purchase in the local area. Since the sensors only read the magnetic field perpendicular to the sensor, the plan was to have three sensors in the center which would measure the magnetic field in the three different axes. However, they will also be affected by the magnetic field generated by the solenoids. In addition to

the center sensors it was planned to have two sets of two sensors between the solenoids. This could be used to make a more advanced observer and to measure the magnetic field generated by the solenoids. This was not done due to damage to some sensors, which required for the spare ones to be used in the center.

5.2.5 Testing of sensors

The datasheet for the hall effect sensors (see Tech N.D) included two different versions of sensors, V1 and V2. These versions had different characteristics. The acquired sensors had no markings to show which version they were, so tests had to be conducted. The tests consisted of accurately measuring a permanent magnetic field at different distances, with the use of an oscilloscope. With the results of the tests it was concluded that the sensors were of the type V1. The V1 sensor has a sensitivity of 2 mV/G [millivolt / Gauss]. The results also showed a variation between 1.7 and 2.3 mV/Gauss, which suggests the sensors were not as linear as documented in the datasheet.

5.2.6 Instrumental amplifiers

Due to the low sensitivity of the sensors, the output voltage was too insufficient to measure all the movements of the levitating magnet. To solve this an Instrumentation Amplifier (In-Amp) was added to the output each sensor. The In-Amp was used to both amplify the sensor signal, and to remove the offset from the magnetic field caused by the permanent magnets. This was done by connecting a potentiometer to the negative input of the In-Amp. When the levitating magnet was in its equilibrium, the potentiometer was adjusted until the two inputs of the In-Amp were equal. This was done for all three hall effect sensors. This gives the following equations:

$$A = 5 + \frac{80k\Omega}{R_g} \quad (5.1)$$

$$V_{out} = A * (V_+ - V_-) + V_{ref} \quad (5.2)$$

Where A is the In-Amp gain and R_g is the In-Amp gain resistor. V_{out} is the In-Amp's output voltage. V_+ and V_- are the input voltages and V_{ref} is the In-Amp's reference voltage.

The Teensy can only input a maximum of 3.3V, meaning the output from the In-Amp needs to be

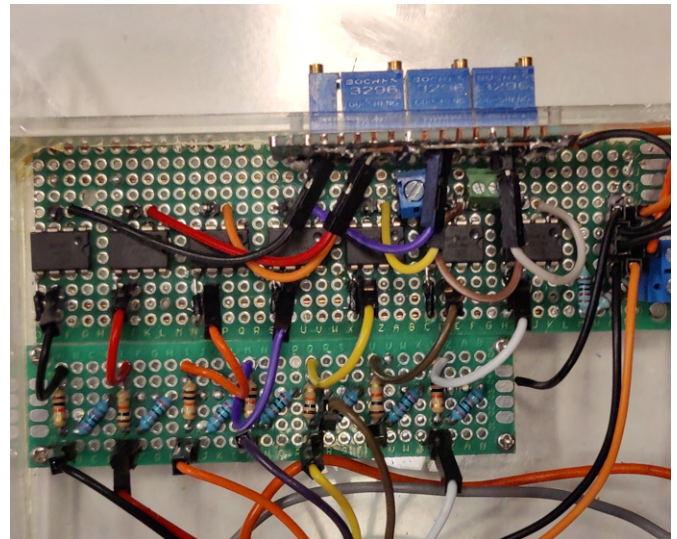
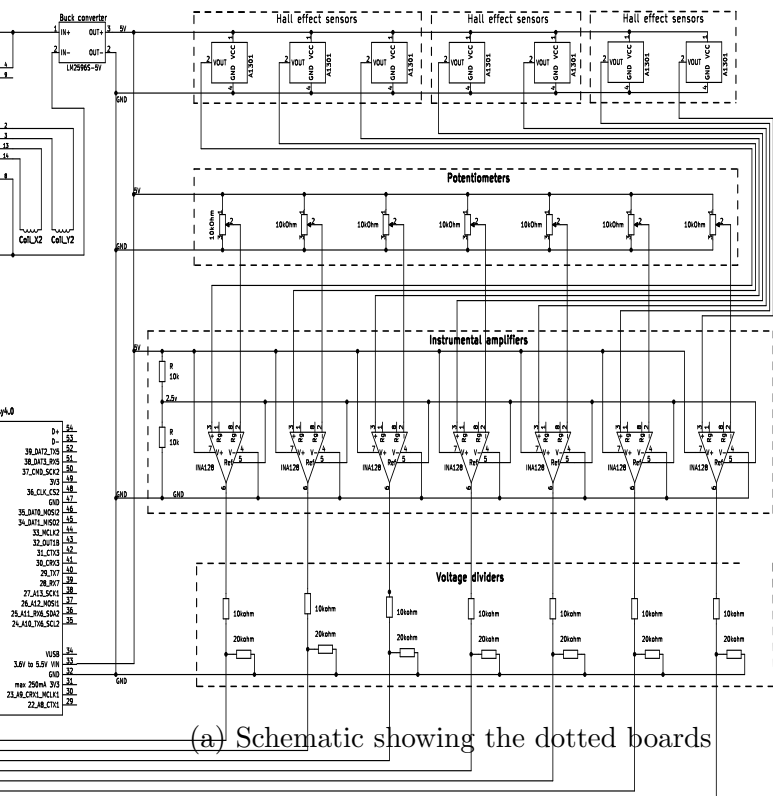
reduced by $\frac{2}{3}$. This was done using a voltage divider circuit. V_{ref} was set to 2.5 V, which means the sensor readings in equilibrium was 2.5V. It will then either increase or decrease depending on the levitating magnets position. Since no resistor is connected the gain is set to 5 ($R_g = \infty$). Thus the input to the controller is:

$$V_{in} = \frac{2}{3} * (5 * (V_{sensor} - V_{pot}) + 2.5V) \quad (5.3)$$

5.3 Results

unnned electrical schematic. The output of the motor
utput to the solenoids were as expected.

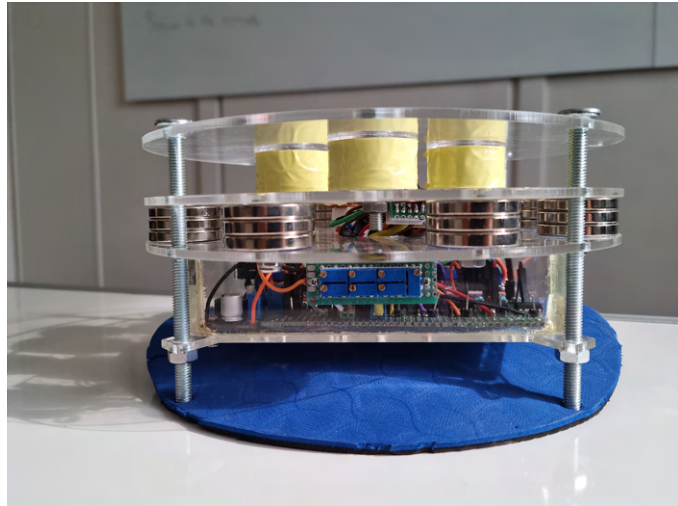
physical boards the components are placed on, shown
wn in figure 5.6b. The full electrical schematic can



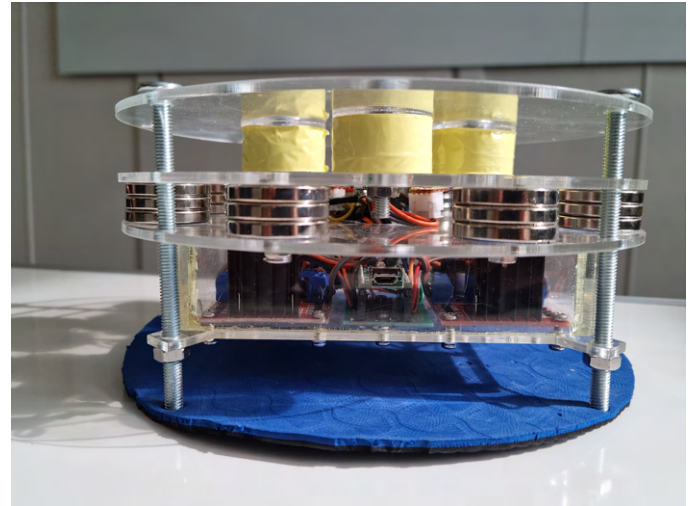
(b) Physical implementation

Figure 5.6: Comparison between the schematic and the physical implementation

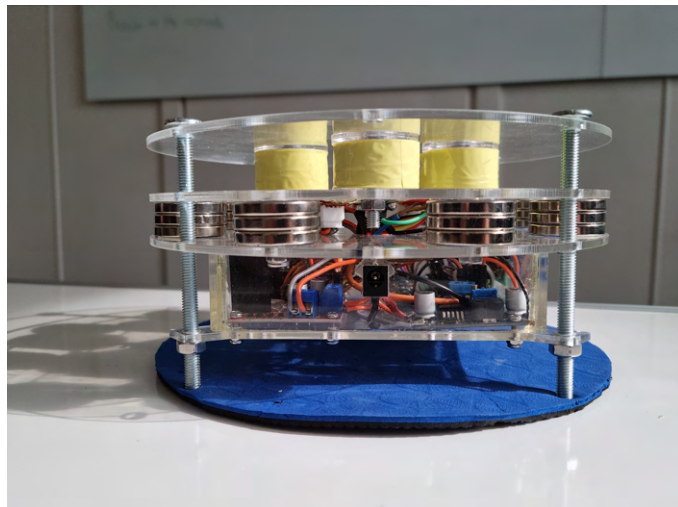
The physical system was made according to the plan. When the DC-jack is plugged in, the system will automatically run its installed code. To install new code, the Teensy can easily be connected to with USB from the outside. The potentiometers can also be adjusted from the outside. The results are shown in figure 5.7



(a) Potentiometer side



(b) Teensy side



(c) DC-Jack side

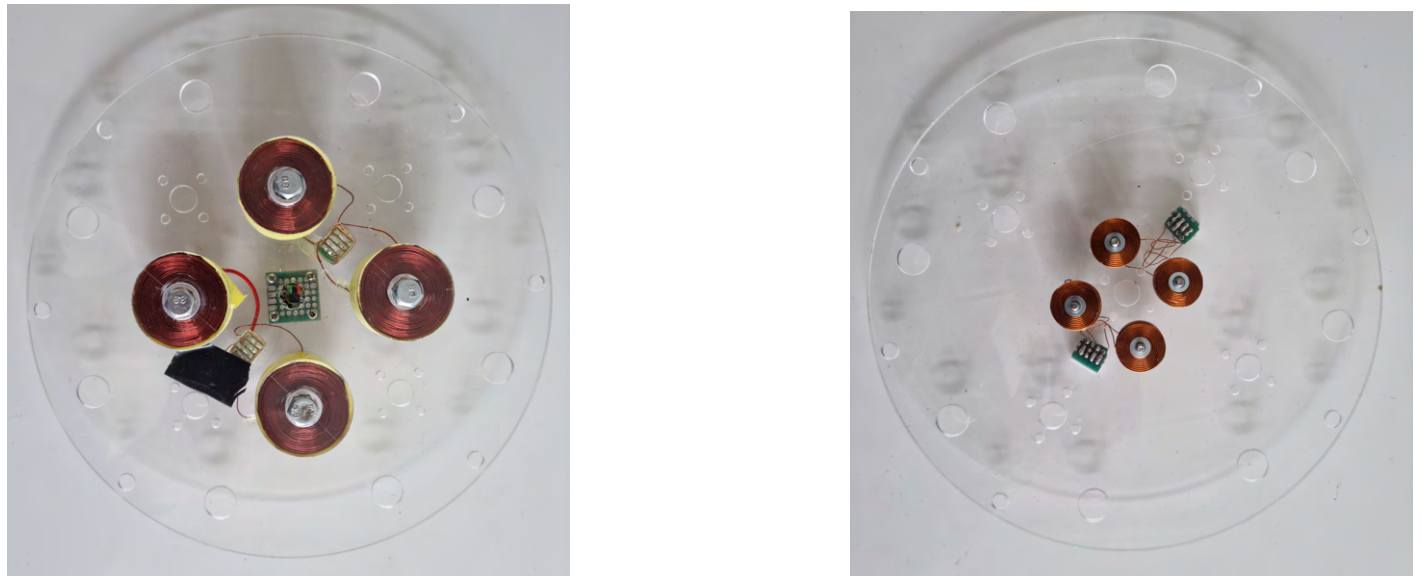


(d) Top

Figure 5.7: Different angles of the finished physical system

5.3.1 Different configurations

Because of the problems stabilizing the system, different configurations were experimented with. Considering the fact that the analog system worked with the current permanent-magnet setup, a configuration was made in which the solenoids (5.8a) were replaced with the smaller electromagnets used in the analog



(a) Original configuration

(b) Analog imitation

Figure 5.8: Different configurations

system(5.8b). The distance between the electromagnets and sensors were also reduced to be the same as the analog system. The comparison of the configurations are shown in figure 5.8.

5.4 Discussion

5.4.1 High temperatures

The system became relatively hot when running for a while. If the system was kept on and the levitating magnet was kept sufficiently away, the controller would give a constant current to the solenoids and this can cause overheating. To prevent overheating of the system in the future, installing a temperature safety sensor would be advised.

5.4.2 Electrical wiring and soldering

During testing the setup had to be opened and changed many times. This caused the 0.5mm^2 wires to bend, causing bad connections and/or causing the wires to break. This was mostly fixed by replacing the pin header connectors with jst-contacts and larger wires.

5.4.3 Soldering

The soldering on many of the boards were not optimal. Many connections were soldered very close to each other and this increased the risk of a short circuit, see figure 5.9. No short circuits happened during the projects span, but bad soldering could result in noise. In future work on the system, a PCB is recommended to better fasten the connection points, reduce the risk of shorts and to potentially reduce noise.

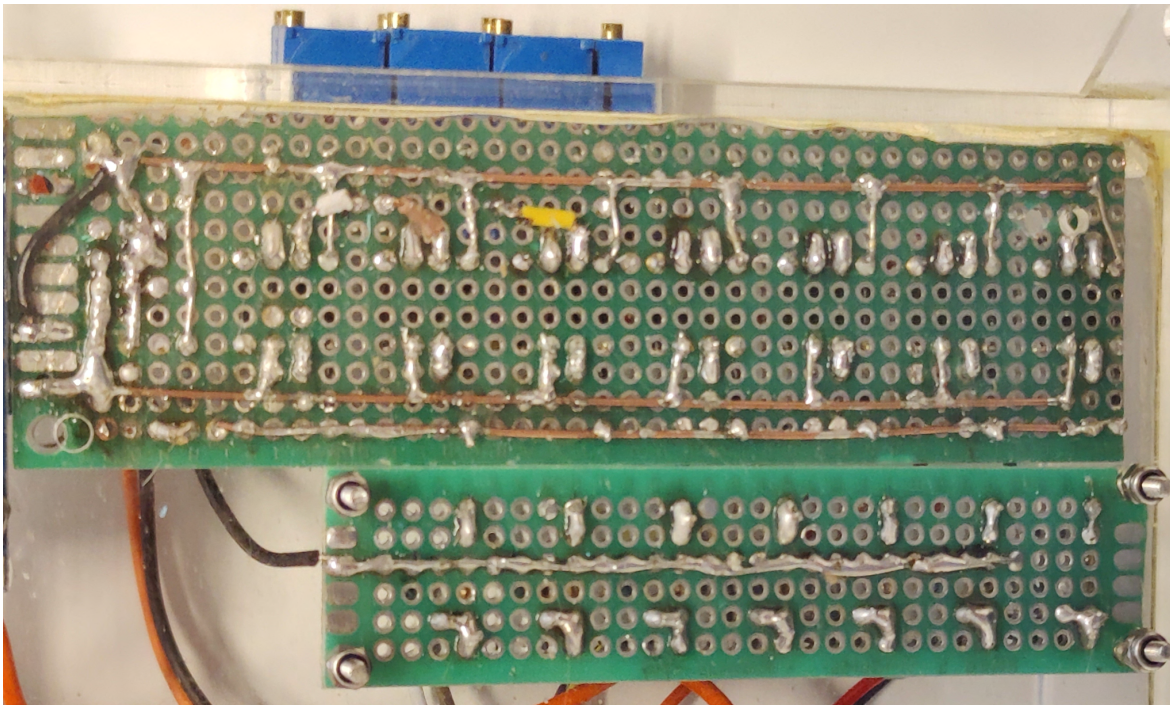


Figure 5.9: Close soldering

5.4.4 Hall effect sensors placement

The hall effect sensors were glued on the protoboard by hand. Both the cutting of the protoboard and the gluing of the hall effect sensors can cause small inaccuracies, see figure 5.5. As the hall effect sensors measure in one direction, they are very sensitive to rotary misplacement. Combining this with the fact that the system operates in a small area with amplified sensor output, inaccuracies may occur. In future works a PCB with hall effect sensors mounted would be recommended.

5.4.5 Damage to the levitating magnet

During the project the levitating magnet got some superficial damage. Every time new controller parameters were tested, the magnet was placed in the center and would eventually fall. The strong

magnetic field could cause the magnet to violently clash with the top plexi-glass plate, and this caused some minor damage to the magnet, see figure 5.10. The potential for damage to the levitating magnet was eventually mitigated by the implementation of a soft mat as a top layer.



Figure 5.10: Damages on the levitating magnet

5.4.6 System modularity

The system was intended to be as modular as possible, not only to make parts easily changeable, but to also to make it easy to try different configurations. A suggestion was multiple mounting holes with different distances for the solenoids. However, due to the coil-wires being very thin this resulted in the wires breaking multiple times when trying to remove/install the solenoids. The solution that was chosen was to have the coil-wires not move at all. To achieve this the coil-wires were soldered to jst-connectors which again was epoxied to the mounting plate. This reduced the wanted modularity of the system. However, it was still possible to change between different solenoid plates with different solenoid distances. Switching between these plates were easy and only required the removal of the five main screws, transferring the wanted sensors and then disconnecting/reconnecting three jst-connectors.

5.4.7 Number of sensors

The original plan for the system was to use seven hall effect sensors, and to implement an observer. However, due to time constraints and inexperience working with observers, the system ended up only

using the three sensors in the center. In addition some sensors were damaged, reducing the number of available sensors. With more sensors one may use a more advanced observer to get more accurate readings. The system is built to support using up to seven sensors, so implementing them would not require much additional work.

5.4.8 Component replacements

Due to some errors during testing some of the components had to be replaced after getting burned out. These include: A Teensy 4.0, and two motor drivers. The three hall effect sensors in the center and their corresponding potentiometer were also burnt. Due to there not being enough replacement sensors and potentiometers at hand, and the fact that the diagonal sensors were not in use, there was made an decision to take the sensors from the diagonal and rather use them in center. So if one wanted to implement the more advanced observer, more sensors needs to be bought.

5.4.9 Solenoid core material

The screws in the solenoids ended up having a major effect on the strength of the magnetic field generated by the solenoids. Due to not having any information about what kind of steel the screws were made of it was quite difficult to figure out the permeability of the core. However, using the screws with the presumed highest permeability added some issues to the system; The levitating magnet was attracted to the screws which would change how the magnetic field behaved. Increasing the permeability of the solenoid cores also added a further delay to the response time of the solenoids.

5.4.10 Noise generated by the solenoids

When the cores of the solenoids had a relative permeability that was approximately 1, the effect that the solenoids had on the the hall effect sensors were quite small. This was when the solenoids core was air. The testing indicated that the maximum effect the solenoids would have on the system readings was approximately 0.6% of the measuring range. This was assumed to be not significant enough to have a noticeable effect on the stability of the system. However when using the smaller electromagnets which were closer to the sensors, the noise increased to an maximum of 10% of the measuring range. This is quite damaging to the sensor readings, making it unable to accurately sense the position of the magnet. To remove this effect there are multiple solutions. First of all the diagonal hall effect sensors could be installed to measure the effect of the solenoids, and then the noise could be removed in the code. On

the other hand a full set of measurements of the different effects of the solenoids depending on the input can be made. This can be linearized to a function for the noise generated and later be removed in the code.

6 Controller design

When being introduced to a plant or process that needs to be controlled, it is important to choose a good strategy for the control structure. There are also different controllers that are suited for different processes. The tuning of the controller itself is important, to get the wanted characteristics. This chapter will therefore describe and discuss the choices that were made in relation to control design.

6.1 Choice of control structure

The microcontroller receives a total of three inputs from the magnetic levitation system. These inputs are the measurement values of three individual hall effect sensors. Each of the sensors reads the magnetic field in the x-, y- and z-axis. As the levitating magnet moves along the xy-plane, the magnetic field in the x- and y-sensors change. The same thing occurs if the levitating magnet moves along the z-axis. The three inputs can therefore be an expression of the position of the magnet.

The microcontroller also contains four outputs, which controls the current in each of the four solenoids. These solenoids are placed along the x- and y-axis. The magnetic levitation platform is therefore a 3×4 -MIMO system, as shown in figure 6.1.

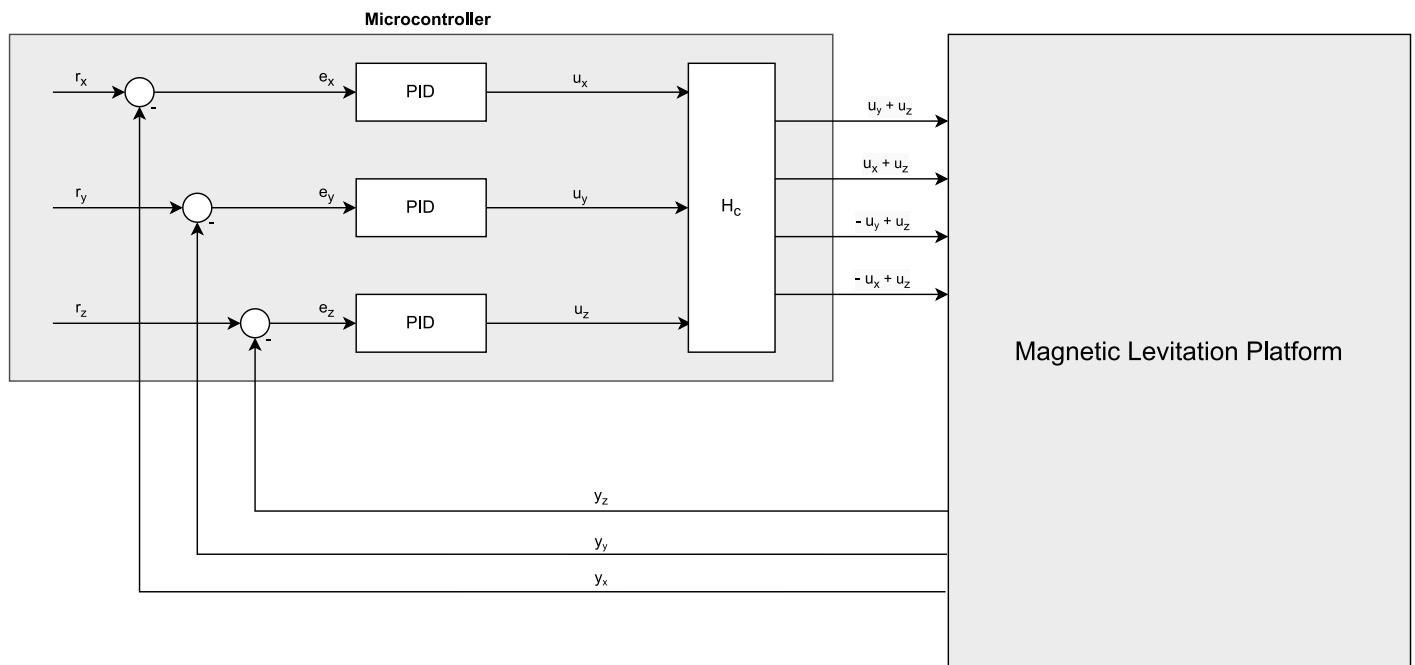


Figure 6.1: Block diagram control structure

Where H_c is the transfer function to the controller. The entire magnetic levitation system is treated as

an unknown transfer function. The readings from the sensors are outputted from this system.

The selected control strategy consists of 3 individual PID-controllers. The reason for this was that it was intended to have 3-DOF, with movement along the x-, y- and z-axis. This has been done by providing each of the controllers with a negative feedback loop. This negative feedback loop is subtracted from the reference in each of the directions, and produces the errors. The errors are then fed into the controllers in each direction, to produce an output in the respective directions. As explained in section 4.6.3 Condition number and RGA this is theoretically a good control structure.

When outputs are applied to the solenoids, the selected strategy was to apply the opposite current along the x- and y-axis. For instance, in the x-axis there are two solenoids, X_A and X_B . If the levitating magnet moved toward one of the solenoids e.g. X_A , it was desired for the closest solenoid (X_A) to push the levitating magnet back towards equilibrium. As well as the opposite solenoid (X_B) to pull. For the levitating magnet to be pushed, it is necessary with a positive current through the solenoid. It is the opposite for pulling, meaning a negative current.

6.2 Digital PID-design

Equation 6.1 shows the continuous PID-equation, which was introduced in section 3.4 *PID-controller*.

$$u(t) = K_p e(t) + K_i \int_0^t e(t) dt + K_d \frac{de(t)}{dt} \quad (6.1)$$

When implementing this controller algorithm into a digital microcontroller, the algorithm needs to be discretized. This was done by substituting t with nT , where

- n = n-th sample
- T = sample time

Since (nT) corresponds to $[n]$, the term $[n]$ will be used forward.

6.2.1 Position form

The proportional term from the continuous pid-equation is shown in equation 3.8. Discretizing this term gives the proportional output, $u_p[n]$:

$$u_p[n] = K_p \cdot e[n] \quad (6.2)$$

The integral term, as shown in equation 3.9, consists of an integral from 0 to t . This can be discretized as a sum from the first sample $n = 1$ to $n - 1$ multiplied by the sample time T . Since the sample time T is assumed to be constant, this term is simplified into K_i .

$$u_i[n] = K_i \cdot \sum_{n=1}^{n-1} e[n] \quad (6.3)$$

Where,

$$K_i = \frac{K \cdot T}{T_i} \quad (6.4)$$

The derivative term includes the derivative of the error as a function of time $\frac{de(t)}{dt}$, as shown in equation 3.11. This can be discretized as Δe divided by T , which is the difference between the current error and the previous error divided by the sample time. The sample time is also here simplified into the K_d gain.

$$u_d[n] = K_d \cdot (e[n] - e[n - 1]) \quad (6.5)$$

Where,

$$K_d = \frac{K \cdot T_d}{T} \quad (6.6)$$

6.2.2 Incremental form

The PID-controller that were used was an incremental PID. An incremental PID uses the differentiation of the proportional, integral and derivative term, to compute the output signal. The incremental algorithm that was used, was derived from the position form. A general incremental output is given as:

$$\Delta u[n] = u[n] - u[n - 1] = \Delta u_p[n] + \Delta u_i[n] + \Delta u_d[n] \quad (6.7)$$

Which gives the output:

$$u[n] = u[n - 1] + \Delta u_p[n] + \Delta u_i[n] + \Delta u_d[n] \quad (6.8)$$

Here, the proportional term is:

$$\Delta u_p[n] = K_p \cdot \Delta e[n] = K_p \cdot (e[n] - e[n - 1]) \quad (6.9)$$

The integral term is:

$$\Delta u_i[n] = K_i \cdot e[n] \quad (6.10)$$

And the derivative term is:

$$\Delta u_d[n] = K_d \cdot (\Delta e[n] - \Delta e[n - 1]) = K_d \cdot (e[n] - 2 \cdot e[n - 1] + e[n - 2]) \quad (6.11)$$

Which all put together gives the full incremental PID-algorithm:

$$u[n] = u[n - 1] + K_p \cdot (e[n] - e[n - 1]) + K_i \cdot e[n] + K_d \cdot (e[n] - 2 \cdot e[n - 1] + e[n - 2]) \quad (6.12)$$

The implementation of this incremental PID-control can be found under the main folder in the GitHub repository ²

6.2.3 Tuning the PID-controller

The magnetic levitation platform is a nonlinear system, which works well with analog control. This is known because of the analog system that was acquired at the beginning of the project. However, since the project is regarding digital control, it was decided to use a digital PD-controller. This was mainly done based on the fact that the controller needed to be as rapid as possible, in order to correct the position of the levitating magnet. The implementation of a PD-controller in the code, meant setting the integral parameter $K_i = 0$.

Since the system is nonlinear, there weren't found any straightforward method of tuning the controllers. It was not possible to use some of the standard methods e.g. the Ziegler & Nichols method or Skogestads SIMC, as explained in 4.7.5 Controller parameters. The parameters for the proportional and derivative gain were therefore found by a systematic trial-and-error method. The best parameters are shown in table 6.1.

²https://github.com/martinbronstad/Bachelor_Thesis_E2207

	K_p	K_i	K_d	Levitation time
PID x	5.2	0	1.0	
PID y	4.2	0	1.0	approx. 20 sec
PID z	2.0	0	0.3	

Table 6.1: PID parameters after tuning

As shown in the table the system was unstable. During testing the system was stable for a couple of seconds before starting to oscillate. The oscillations then got bigger, until the levitating magnet eventually fell towards one of the permanent neodymium magnets. The longest time period for which the levitating magnet levitated only by the power of the magnetic field was approximately 20 seconds.

6.3 Microcontroller settings

The microcontroller that was used was a Teensy 4.0. This was mainly chosen because of its speed, as well as the fact that it runs Teensyduino which is a plugin for the Arduino IDE. There are several settings on the Teensy itself that can be changed, to fit different purposes. Some settings were left on default values, and some were change to fit the system. This section will give an overview of the choices that were made.

6.3.1 ADC

Some settings on the Teensy were adjusted specifically to make the system run more smoothly. Regarding the sensor reading, the ADC was set to 10 bit reading resolution. This was due to the 12 bit reading having more noise, and further slowed down the system. This is also shown in the microcontrollers datasheet (see Semiconductors 2019, page 64), as it shows that the number of effective bits are 10,7. To further decrease the noise, the read averaging was set to 4. This meant the controller reads the sensor data four times and takes a mean of this data before giving an input to the program. A comparison of a 10 bit reading and a 12 bit reading, with averaging set to 4, is shown in figure 6.2.

6.3.2 PWM

The default setting of a Teensy 4.0 is a PWM frequency at 4482 Hz (PJRC 2022). However, the controllers total run time was at around 62 micro seconds. This was measured using simple time

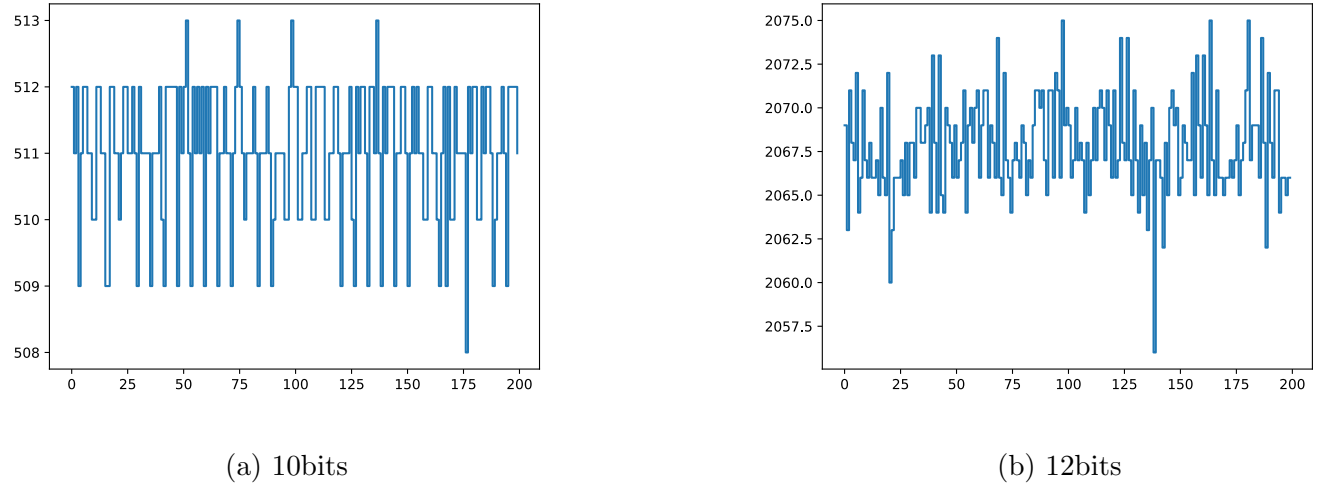


Figure 6.2: ADC analysis with averaging set to 4

functions in the code. Using the formula for frequency, it means the system could send out different outputs at around 16 129 Hz. The formula for frequency is given by:

$$f_s = \frac{1}{T} = \frac{1}{62 \cdot 10^{-6}} \approx 16129 \text{ Hz} \quad (6.13)$$

Where f_s is the sampling frequency, and T is the sample time. Due to this speed discrepancy, the frequency of the PWM signal was turned up to 32 258 Hz. The PWM was not increased higher than this due to the motor drivers having a limitation at 40 kHz.

6.4 Sensor readings

The code for the sensor readings are based on reversing the formula from equation 5.3, to get the difference in Gauss from the set point. To make the computing faster this is done in two steps. The constants can be found in section 5.2.5, and 5.2.6

The calculations from the 10 bit data to mV can be combined with the voltage splitter, so the rest of the calculations can assume everything runs on 5 V. First, all the constants are inverted and combined.

$$10bit \rightarrow mV^{-1} = \frac{3333.3333}{1024} * \frac{3}{2} = \frac{5000}{1024} \quad (6.14)$$

$$Sensorsensitivity^{-1} = \frac{1}{2} \quad (6.15)$$

$$InampAmplification^{-1} = \frac{1}{5} \quad (6.16)$$

$$V_{constant} = \frac{5000}{1024} * \frac{1}{2} * \frac{1}{5} \quad (6.17)$$

$$V_{constant} = \frac{5000}{10240} \quad (6.18)$$

Then the 2.5 V offset is removed. Due to first step amplifies the signal with $V_{constant}$, some constants has to be multiplied to the V_{offset} as well.

$$V_{offset} = 2500 * \frac{1}{2} * \frac{1}{5} \quad (6.19)$$

$$V_{offset} = 250 \quad (6.20)$$

$$\Delta G = Sensordata \cdot V_{constant} - V_{offset} \quad (6.21)$$

6.4.1 Noise analysis

Due to the high speed of the readings, there had to be made an external program to measure and analyse the noise. The program worked by taking data from the readings and time from the serial monitor of the Arduino IDE. This was put through a python script to be analysed. The script first verifies that the data is not corrupted, by checking if the time between the readings are stable. Then it measures the time difference between the noise peaks.

The results from this analysis (figure 6.2a) shows that when the 10 bit ADC is running with an averaging set to 4, the noise have small peaks that average to 3030 Hz and some bigger ones which averages to 133 Hz. However, the noise has a total amplitude at around 4 bits, which is only 0.4% of the effective measuring range. This is not that impactful when considering the fact that the ADC does have a maximum error of 1 bit.

The 12 bit adc (figure 6.2b) has a more visible oscillating behaviour, but the noise has a total amplitude at around 18 bits. This is about 0.44% of the effective measuring range. This is not that much higher

in effective measuring range compared to the 10 bit analysis (figure 6.2a). The main difference between the 10 bit and 12 bit is therefore the behaviour of the noise, the sample speed, and the sensitivity of the readings.

6.4.2 Filter design

The input readings from the sensors contain noise. It was therefore needed to filter this noise out, in order to have as accurate readings as possible. Two different filters were implemented to see what kind would fit the system; A Lowpass filter (LinnesLab 2020), and a Simple Kalman filter (denyssene 2020).

The tests are shown in figure 6.3. These show that the LP filter might have more stable readings, but it also adds a delay of approximately 100 samples. This is equivalent to a delay of 5.2 milliseconds. Which could be detrimental towards the control of the system. Both filters have been used for further tests to determine the effect they have on the stability.

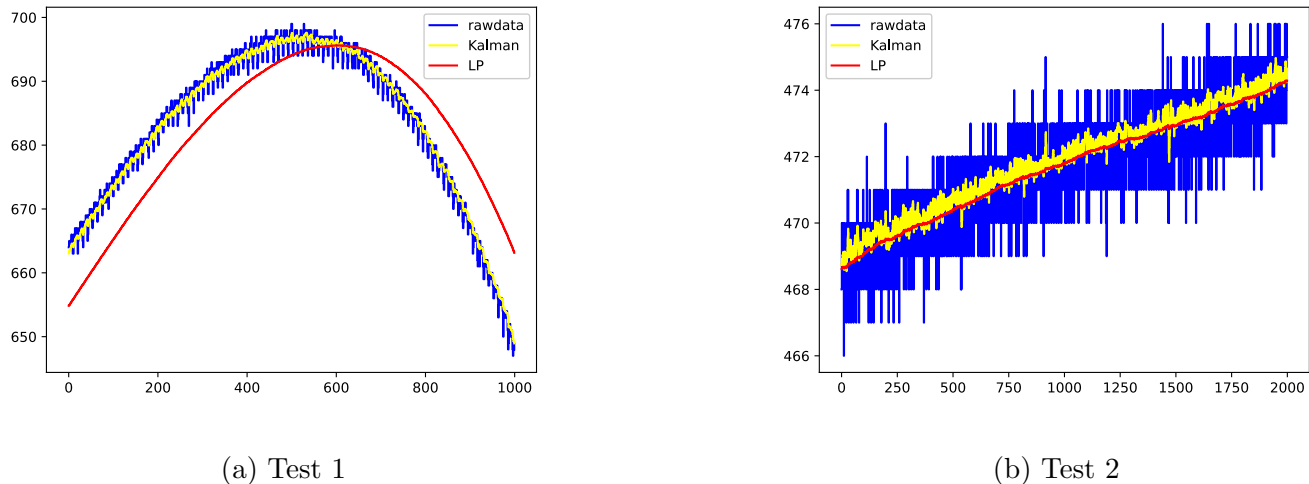


Figure 6.3: Filter analysis

6.5 Output algorithm

As mentioned in section 6.1 *Choice of control structure* the microcontroller consist of 3 individual PID-controllers. Each controller computes an output for each of the directions, hereunder u_x , u_y and u_z . These three outputs needs to be sent to the correct motor drivers to power the correct solenoids.

This was done by implementing two different functions in Arduino IDE. These two functions works exactly the same, but along different axes. The "*Turn X*" function controls the solenoids along the x -axis, and "*Turn Y*" controls the solenoids along the y -axis. These functions gets sent their respective u_x and u_y , and in addition they both also receive u_z . Before the outputs are sent to the functions, they are saturated. The output along the x - and y -axis are saturated to the minimum and maximum value the microcontroller can send out. The reason for this was to make sure that the solenoids had a greater controllability along the xy -plane. The z -output was saturated to approximately 40% of the maximum output, in order to make the effects of the x and y controllers greater. The saturations are shown in table 6.2.

Output	Minimum value	Maximum value
u_x	-255	255
u_y	-255	255
u_z	-100	100

Table 6.2: Output saturations

When the outputs were received in the functions, they were first summarized based on the different solenoids. As shown in the block diagram in figure 6.1 the solenoids received the opposing outputs along the same axes. In addition, all of the solenoids received an additional output from the z controller. The different solenoids therefore received the outputs shown in table 6.3.

Solenoid	Output
X1	$u_x + u_z$
X2	$-u_x + u_z$
Y1	$u_y + u_z$
Y2	$-u_y + u_z$

Table 6.3: Outputs to different solenoids

These sums were then saturated, to make sure that the output that was sent to a motordriver was never greater than ± 255 . However, the Teensy can not output any negative values. The Teensy can only output PWM-signals between 0 and 255. This was solved as shown in figure 6.4. The sum that was going to be outputted to a motordriver, were put through an if statement. If $0 \leq u_{solenoid} \leq 255$

then the Teensy firstly sets the motor driver in a "direct" mode. This was done using logical low/high pins, to make the motor driver send current positively through the solenoid. $u_{solenoid}$ was then sent as a PWM-signal to the motor driver via `analogWrite`.

If the sum was negative, $-255 \leq u_{solenoid} < 0$, then the motor driver would be "reversed". This makes the motordriver flip the polarity, and send negative current through the solenoid. $u_{solenoid}$ was then inverted via an absolute value function, to get the corresponding positive value. This value was then outputted to the motor driver via `analogWrite`.

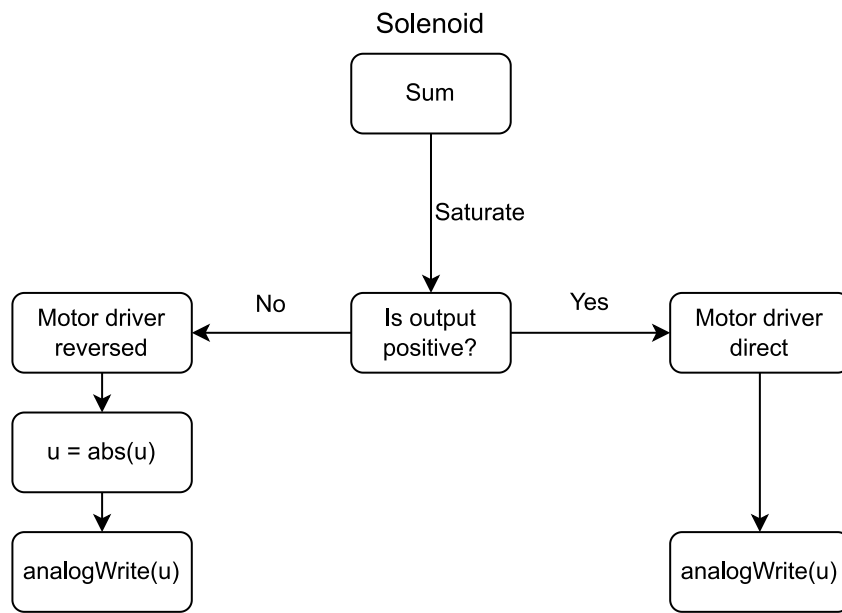


Figure 6.4: Output logic in a flow diagram

6.6 Discussion

6.6.1 Stabilisation issues

During the development of the output algorithm, there were some versions of the code that worked better - and some that worked worse.

The version of the code that worked the best in regards of stabilisation, turned out to be a sort of on/off-controller. The reason this occurred was due to a bug in the saturation of the output signals. There were certain situations in which the code could send negative values to the motor drivers. However, the Teensy cannot output any values below 0, as explained in subsection 6.5 *Output algorithm*. An example of what is really outputted when a negative value is sent to `analogWrite` is shown in figure 6.5.

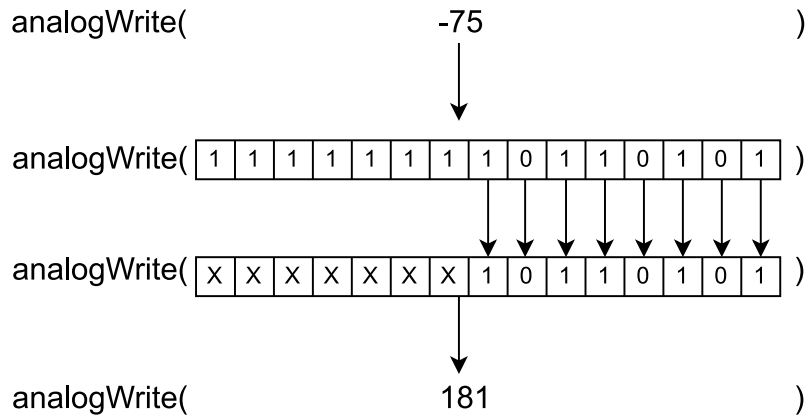


Figure 6.5: Bit manipulation

In this example a negative value of -75 is sent to `analogWrite`. The outputs were defined as integers, which consists of 16 bits. The negative numbers are represented by two's complement binary (Arduino 2019). The corresponding bit register for -75 is shown in the second line. However the `analogWriteResolution`, which is the number of bits that can be written, was set to 8. This means the `analogWrite` function only reads the 8 last bits as shown in the third line. The bit value of "1 0 1 1 0 1 0 1" corresponds to an output of 181 (71% duty cycle). *Figure 6.6* shows the output that was sent to the solenoids, via the motor drivers. As shown this is essentially an on/off-controller.

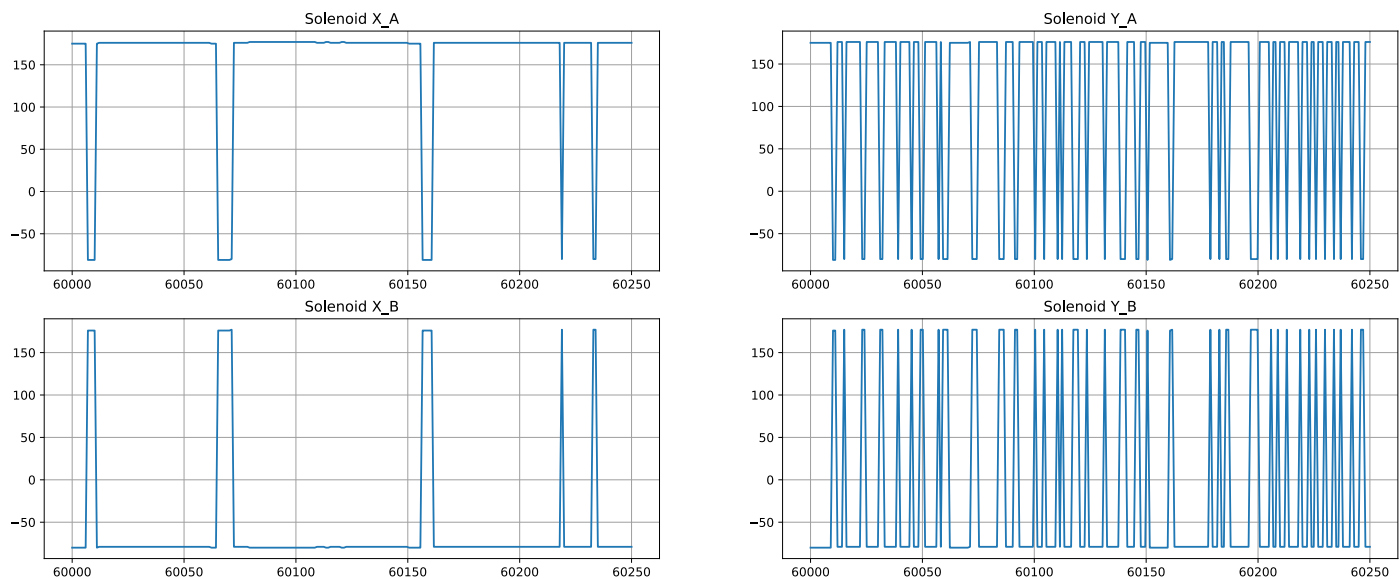


Figure 6.6: On/off control of the solenoids

6.6.2 Output algorithm

As mentioned in ?? ?? the system became more stable when it sent out non-intended outputs. Figure 6.7 shows what the output that was sent from the Teensy was. This figure shows the plot in the time period $3.5sec \leq t \leq 4.0sec$ after the logging was started. This is therefore during a period in which the levitating magnet was stabilized for some time.

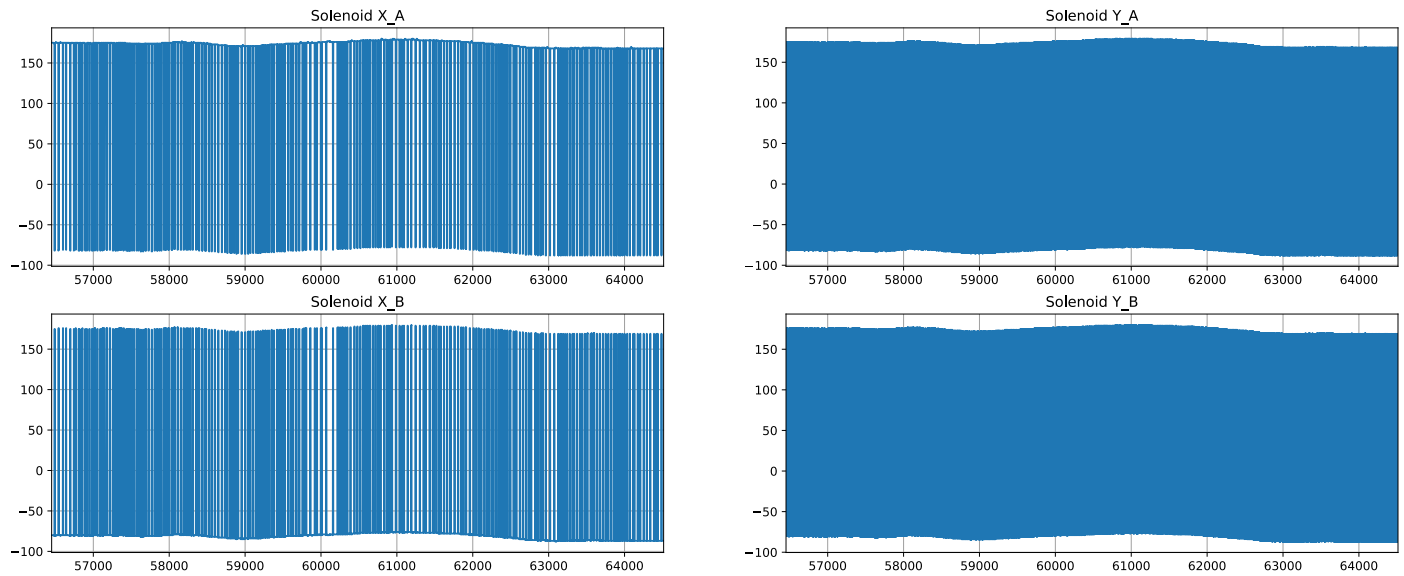


Figure 6.7: Output values from the Teensy 3.5 seconds to 4.0 seconds, plotted in Python

However, it was wanted to analyse the actual current in the solenoids. This was simulated based on an estimated transfer function of the solenoid, with the transfer function given by (Electrical4U 2020). The transfer function was estimated based on a RL circuit, since the solenoid has an internal resistance and inductance. The solenoids resistance was measured physically with an ampere meter, and was measured to 14ohm . The inductance was calculated to $0,604\text{H}$. The transfer function from the input voltage V_{in} to the solenoid current $I(s)$ is given by

$$I(s) = \frac{V_{in}(s)}{R + L \cdot s} \quad (6.22)$$

The input voltage is constantly 10.3V DC as given in 5.2.3 Motor drivers. This gives the transfer function

$$I(s) = \frac{10.3}{14 + 0.604s} \quad (6.23)$$

It was simulated a simple step in order to verify the transfer function. Considering the solenoids have

$L = 0.604H$ and $R = 14\text{ohm}$, the time constant τ is given by

$$\tau = \frac{L}{R} = \frac{0,604H}{14\text{ohm}} = 0,04314s = 43,14ms \quad (6.24)$$

As shown in figure 6.8, the step response reaches approximately 63% of its final value at 43ms. At the time $t = 0.043$ it reaches 0.465, which is 63.18% of its final value 0.736. This is close enough to 63.2% which is a verification of the transfer function for the solenoid.

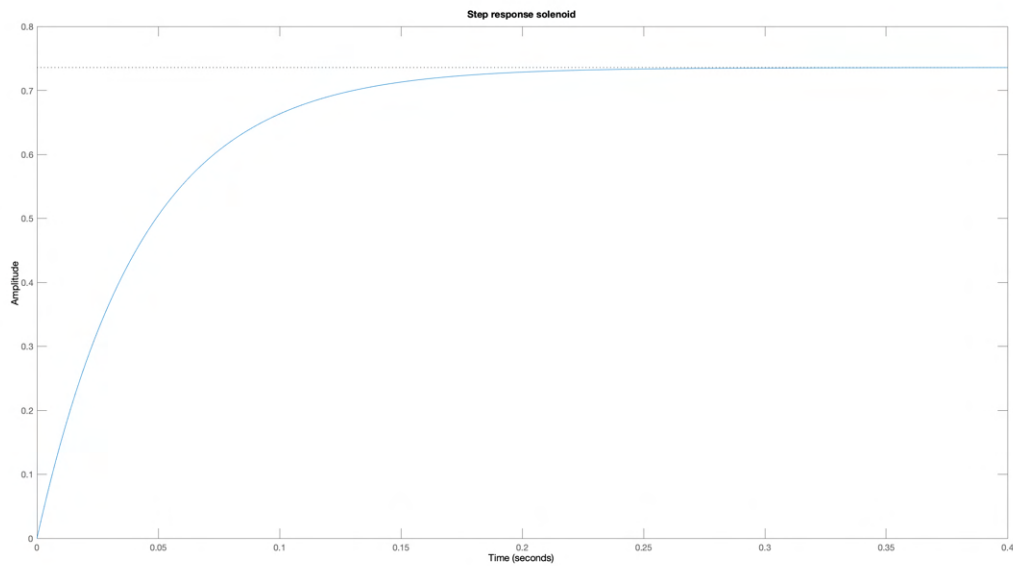


Figure 6.8: Step response of the solenoid

In order to simulate the actual current of the solenoid, the output data given in figure 6.7 had to be applied to the solenoids. The output data was therefore divided by 512 and multiplied by the transfer function of the solenoids. It was divided by 12 in order to translate an 8-bit value, to a value up to $\pm 0.5A$ as this was the measured maximum and minimum current in the solenoids. This gives the following function of the simulated current in the solenoids:

$$I_{\text{solenoids}} = (\text{outputdata}/512) \cdot \frac{12}{14 + 0.604s} \quad (6.25)$$

The simulated current in each of the four solenoids are shown in figure 6.9. The grayed out lines are the values from the Teensy, and the blue lines are the values from the simulated current. As shown in the figure, the solenoids actually generates a varying bias current. The first solenoid X_A produces a current

around 0. In comparison the opposite solenoid X_B generates a current of around 0.2A. The solenoids along the y-axis creates a bias current as well. Solenoid Y_A generates a current of around -0.14A to -0.13A, and solenoid Y_B generates a current between 0.28A and 0.30A. This means neither X-solenoids or Y-solenoids are linear around 0. Their middle value are

$$I_{x,mid} = \frac{0.2A + 0A}{2} = 0.1A \quad \& \quad I_{y,mid} = \frac{0.29A + (-0.135A)}{2} = 0.078A \quad (6.26)$$

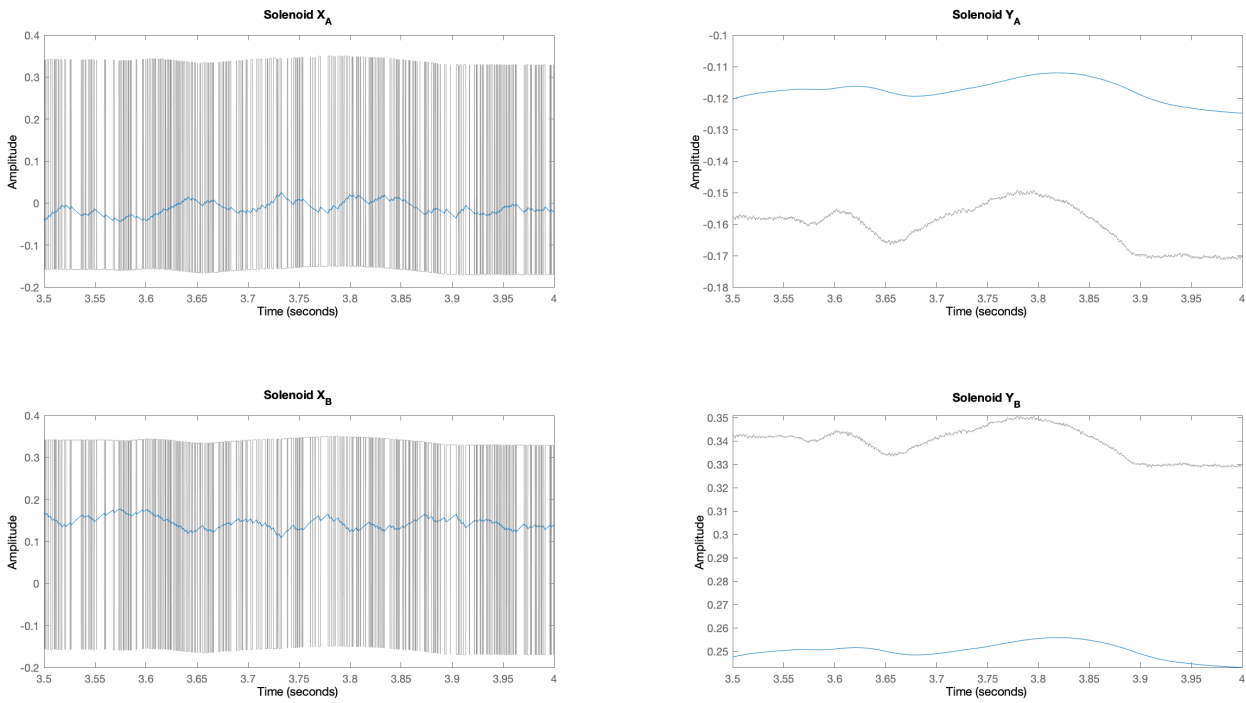


Figure 6.9: Simulated actual current in the solenoids [A].

One reason as to why this was stable might have been because of the position of the levitating magnet. The equilibrium in which the magnet levitated, was never centered in the middle of the solenoids. The different equilibriums were always a bit outside of the "origo" along the xy-axis, meaning the permanent magnets pulled more towards the magnet in e.g. the negative or positive x- and y-axis. Along with solenoids that are pushing more along the opposite x- and y-axis, this might have created an unstable equilibrium in which the sum of the forces were close to zero.

If the sum of forces is close enough to zero, the levitating magnet may appear to be stable for some time. Then oscillations start because it is an unstable equilibrium, the sum will oscillate between bigger

and bigger values, until it eventually falls off.

When the issue with the output algorithm was resolved and the algorithm described in subsection 6.5 *Output algorithm* was implemented, the system became more unstable. The reason for this might be that the solenoids were not strong enough and/or not receiving a varying enough current. However, due to time limitations during the testing period this was never tested properly.

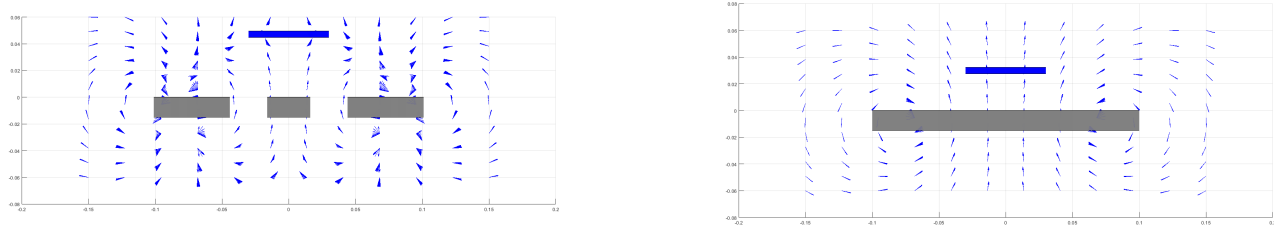
6.6.3 Permanent magnetic field

Another factor to the destabilization might be the permanent magnetic field. As explained above the levitating magnet was never stable in "origo", but rather a bit off. Figure 6.10 is a comparison of the magnetic fields from the permanent magnet in the chosen setup (figure 6.10a) compared to the analog system (figure 6.10b). As the figure shows, the magnetic field vectors point a bit differently in equilibrium. In the analog system shown at the bottom, the field vectors are pointing up almost vertically. In comparison, the neodymium setup has magnetic field vectors pointing more horizontally upwards.

In addition the analog setup had a magnetizable material in the core of the electromagnets, which essentially pulls the levitating magnet downwards towards the center of the electromagnets. This creates a more rigid operating point. This is because of the permanent magnetic field pushing the levitating magnet more or less upwards and a bit outward, while the levitating magnet itself pulls downwards and a bit outward towards the electromagnets core. In comparison the chosen setup consist of solenoids, and a more horizontally permanent magnetic field. As explained in subsection 3.1.5 Solenoids, solenoids use a non-magnetized core. This creates a less rigid operating point, as the solenoids themselves will have to pull and push more to keep it stable.

6.6.4 Two dimensional control

During the testing and development period, it was tested with only two controllers instead of three. Meaning excluding the z-controller, and only focusing on the stabilisation of a two dimensional system. There were no difference in how unstable it was, whether it was with or without the z-controller. This might be because of the same reason as mentioned in the paragraph above, a non optimal configuration. In hindsight, a good idea would be to focus on two-dimensional control and stabilisation before moving toward control along the z-axis.



(a) Neodymium magnet

(b) Ring magnet

Figure 6.10: Comparison of simulated permanent magnetic fields

6.6.5 State observer

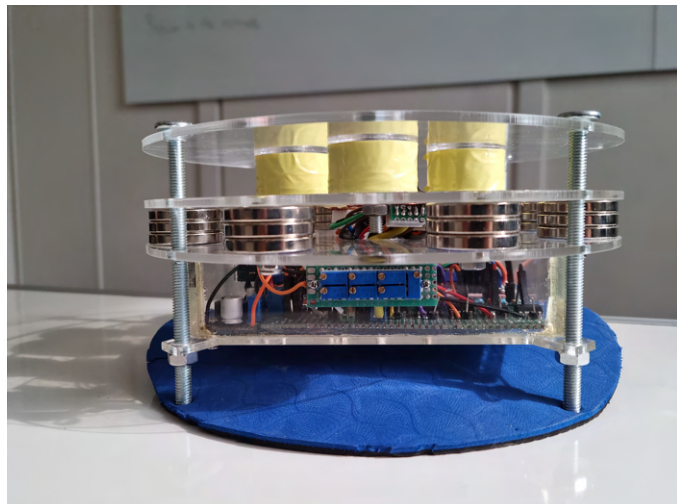
There is reason to think that implementation of a state observer would greatly improve the control performance of the system. With the current 3-sensor setup the rotation of the levitating magnet has a big impact on the sensor readings, making it difficult to control the x-, y- and z-position of the magnet. Full state feedback would also allow for the implementation of and LQR controller which for a MIMO system like this might perform better than PID.

7 Results

The link below shows a video of the system levitating the magnet for approximately 15 seconds. The magnet starts off fairly stable, but then starts slowly oscillating more and more until it falls down.

<https://www.youtube.com/watch?v=oAsrtkBLMx4>

The resulting physical system is shown in figure 7.1. It consists of laser cutted plexi-glass layers, including an electrical housing made from plexi-glass. The lower layer is the electrical housing including the electrical components. The middle layer consists of 8 groups of neodymium magnets, in stacks of 3, which generated the permanent magnetic field. The top layer consists of the solenoids, with three hall effect sensors placed in the middle. Above the top layer a protection plexi-glass plate is secured. All the layers are fastened to each other using screws and bolts. The system was built and functioned as designed. The system is easy to use as both the potentiometers and the Teensy is accessible from the outside, without taking the system apart.



(a) Potentiometer side



(b) Top

Figure 7.1: Different angles of the finished physical system

8 Discussion

The process of designing, building and controlling a magnetic levitation platform is a fairly involved process with a lot of moving parts. There are many reasons why the system is currently unstable, most of which has already been discussed in the previous sections of the report. However, we would also like to highlight time and money constraints as contributing factors. In hindsight we should have spent more time researching, simulating and getting to know the model before designing the new system, but due to the time sensitive nature of ordering components this stage was a little rushed. Low budget also meant choosing lower quality electrical components such as sensors, potentiometers and power supply, which again lead to the system being less reliable. Having a less reliable system ultimately meant not being able test everything systematically.

8.1 Future work

As discussed in the previous sections of the report there are many areas of the project that can be improved upon in the future. To summarize, the most important ones are:

- Implementation of state observer
- Testing out different permanent magnet setups
- Experimenting with adding extra resistance to the solenoid circuit.
- Implementation of PCB
- Better cables and cable connections
- Better sensors
- More accurate sensor placement
- More accurate potentiometers

9 Conclusion

The main goals of this project, as described in section 1.2, was to design, prototype and build a magnetic levitation platform with a digital PID controller.

The work with modelling the physical components went more or less as planned. The model was expanded to suit the new system, and a simulation framework was built to test both different magnet and controller configurations. Due to inexperience with both Matlab and magnetic levitation, more time and resources were spent researching than expected. The linear analysis did not go as planned, and unfortunately no reasonable controller parameters were found from it.

The prototype was functional and built as planned. However, in hindsight there are several factors that could be improved. The system was about as modular as planned, but many of the connectors and wires to the movable parts did not handle the strain of repeated bending and usage. This could cause bad connections and required more time than anticipated to diagnose and repair. Possible inaccuracies might have occurred due to poor quality of many of the components.

The controller did not meet the requirements set initially, as it didn't stabilize the system. This was due to a number of factors, including an unexpectedly large time delay in the solenoids, a weaker magnetic field than expected and a permanent magnetic field with a much less rigid equilibrium than desired.

In conclusion the system ended up being functional, but not stable. Based on the analysis of the current system there is reason to believe that a stable version could be achieved further down the line with more tests, fixes and improvements. Although a lot of the initial goals were either reached or partly reached, there is still a lot of room for improvement in all aspects of the system, both in terms of the mathematical framework and on the physical system. Hopefully the resulting system will be improved upon in future projects.

It is safe to say we as a group underestimated how complex and time consuming this project would become, but we view it as an invaluable learning experience.

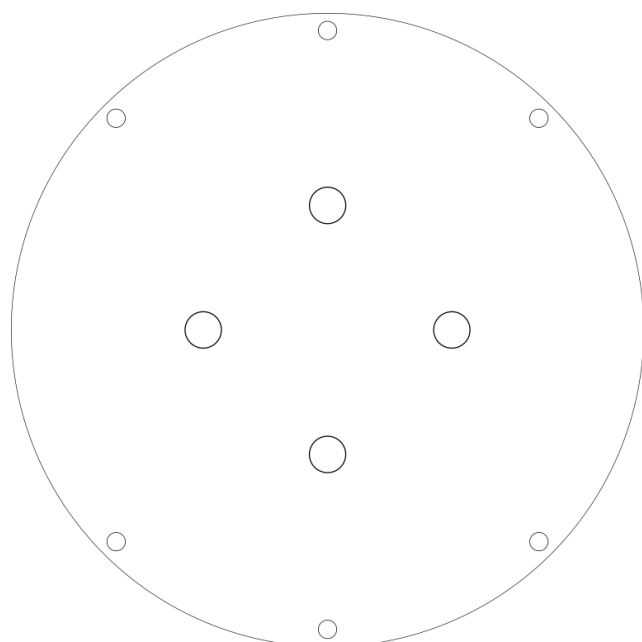
References

- [1] ABLIC. *What is an Operational Amplifier?* <https://www.ablic.com/en/semicon/products/analog/opamp/intro/> (Accessed: 12.05.2022). no date.
- [2] AliExpress. *load 500g Magnetic levitation core band LED lamp Magnetic levitation module Magnetic levitation naked system High-tech with LED.* <https://www.aliexpress.com/item/32845962420.html?gatewayAdapt=glo2deu> (Accessed: 17.05.2022). N.D.
- [3] T. Andresen, J.G. Balchen and B.A. Foss. *Reguleringssteknikk.* Institutt for teknisk kybernetikk, NTNU, 2016.
- [4] Arduino. *ints.* <https://www.arduino.cc/reference/en/language/variables/data-types/int/> (Accessed: 12.04.2022). 2019.
- [5] Anna Binnie. “Using the history of electricity and magnetism to enhance teaching”. In: *Science & Education* 10.4 (2001). <https://doi.org/10.1023/A:1011213519899> (Accessed: 18.05.2022).
- [6] E. Bristol. “On a new measure of interaction for multivariable process control”. In: *IEEE transactions on automatic control* 11.1 (1966), pp. 133–134.
- [7] Chegg. *Poles Of A Magnet.* <https://www.chegg.com/learn/physics/introduction-to-physics/poles-of-a-magnet> (Accessed: 13.05.2022). no date.
- [8] David Cook. *Cutting Open a Trimming Potentiometer.* <http://www.robotroom.com/Trimpots-2.html> (Accessed: 17.05.2022). N.D.
- [9] denyssene. *Simple Kalman Filter Library.* <https://github.com/denyssene/SimpleKalmanFilter> (Accessed: 18.05.2022. 2020).
- [10] R. Doshmanziari, H.A. Engmark and K.T. Hoang. *Maglev model description.* https://folk.ntnu.no/hansae/Maglev_System_Description.pdf (Accessed: 13.05.2022). 2021.
- [11] Electrical4U. *RL Circuit Transfer Function Time Constant RL Circuit as Filter.* <https://www.electrical4u.com/rl-circuit-transfer-function-time-constant-rl-circuit-as-filter/> (Accessed: 10.05.2022). 2020.
- [12] ElectronicsTutorial. *Hall Effect Sensor.* <https://www.electronics-tutorials.ws/electromagnetism/hall-effect.html> (Accessed: 13.05.2022). no date.
- [13] J. Fraden. *Handbook of Modern Science: Physics, Design and Application.* https://books.google.no/books?id=WOEmv9dAJ1kC&q=%22neodymium+magnet%22+strongest&pg=PA73&redir_esc=y#v=snippet&q=%22neodymium%20magnet%22%20strongest&f=false (Accessed: 13.05.2022). 2010.

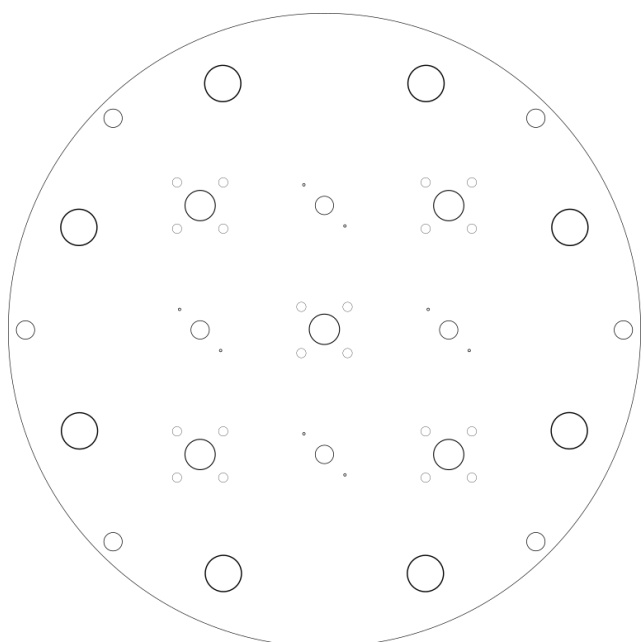
- [14] Funilab. *Arduino Air Bonsai Levitation*. <https://www.instructables.com/Arduino-Air-Bonsai-Levitation/> (Accessed: 12.04.2022). 2018.
- [15] A.K. Ghosh. *Introduction to measurements and instrumentation, 4th ED*. Prentice Hall India Learning Private Limited, 2012.
- [16] M.A. González and D.E. Cárdenas. “Analytical Expressions for the Magnetic Field Generated by a Circular Arc Filament Carrying a Direct Current”. In: *IEEE Access* 9 (2020), pp. 7483–7495. DOI: 10.1109/ACCESS.2020.3044871.
- [17] C. Grimholt and S. Skogestad. “Optimal PI and PID control of first-order plus delay processes and evaluation of the original and improved SIMC rules”. In: *Journal of Process Control* 70 (2018), pp. 36–46. ISSN: 0959-1524. DOI: <https://doi.org/10.1016/j.jprocont.2018.06.011>. URL: <https://www.sciencedirect.com/science/article/pii/S0959152418301252>.
- [18] W Jones. “Earnshaw’s theorem and the stability of matter”. In: *European Journal of Physics* 1.2 (Apr. 1980), 85–88. <https://doi.org/10.1088/0143-0807/1/2/004> (Accessed: 06.05.22). DOI: 10.1088/0143-0807/1/2/004. URL: <https://doi.org/10.1088/0143-0807/1/2/004>.
- [19] C. Knospe. “PID control”. In: *IEEE Control Systems Magazine* 26.1 (2006), pp. 30–31.
- [20] LinnesLab. *KickFiltersRT*. <https://github.com/LinnesLab/KickFiltersRT> (Accessed: 18.05.2022. 2020).
- [21] Motoharu Ono, Shunsaku Koga and Hisao Ohtsuki. “Japan’s superconducting Maglev train”. In: *IEEE Instrumentation & Measurement Magazine* 5.1 (2002). <https://doi.org/10.1109/5289.988732> (Accessed: 18.05.2022).
- [22] PJRC. *Teensyduino, Pulsed Output: PWM & Tone*. https://www.pjrc.com/teensy/td_pulse.html (Accessed: 06.05.22). 2022.
- [23] D. E. Seborg et al. *Process Dynamics and Control*. Wiley, 2016, pp. 331–338.
- [24] NXP Semiconductors. *i.MX RT1060 Crossover Processors for Consumer Products*. https://www.pjrc.com/teensy/IMXRT1060CEC_rev0_1.pdf (Accessed: 20.04.2022). 2019.
- [25] S. Skogestad and I. Postlethwaite. *Multivariable Feedback Control*. Wiley, 2007.
- [26] Sparkfun. *L298 Dual full-bridge driver datasheet*. https://www.sparkfun.com/datasheets/Robotics/L298_H_Bridge.pdf (Accessed: 20.04.2022). 2000.
- [27] Yangzhoi Positioning Tech. *49E Hall-effect linear position sensor data sheet*. <https://p.globalsources.com/IMAGES/PDT/SPEC/440/K1139513440.pdf> (Accessed: 20.04.2022). N.D.

- [28] WikimediaCommons. *Op-Amp Differential Amplifier*. https://upload.wikimedia.org/wikipedia/commons/a/a2/Op-Amp_Differential_Amplifier.svg (Accessed: 16.05.2022). 2009.
- [29] WikimediaCommons. *Op-Amp Instrumentation Amplifier*. https://commons.wikimedia.org/wiki/File:Op-Amp_Instrumentation_Amplifier.svg (Accessed: 16.05.2022). 2009.
- [30] WikimediaCommons. *Opampvoltagefollower*. <https://upload.wikimedia.org/wikipedia/commons/d/d2/Opampvoltagefollower.svg> (Accessed: 16.05.2022). 2006.
- [31] Hamid Yaghoubi. “The most important maglev applications”. In: *Journal of Engineering* 2013 (2013). <https://www.hindawi.com/journals/je/2013/537986/> (Accessed: 18.05.2022).

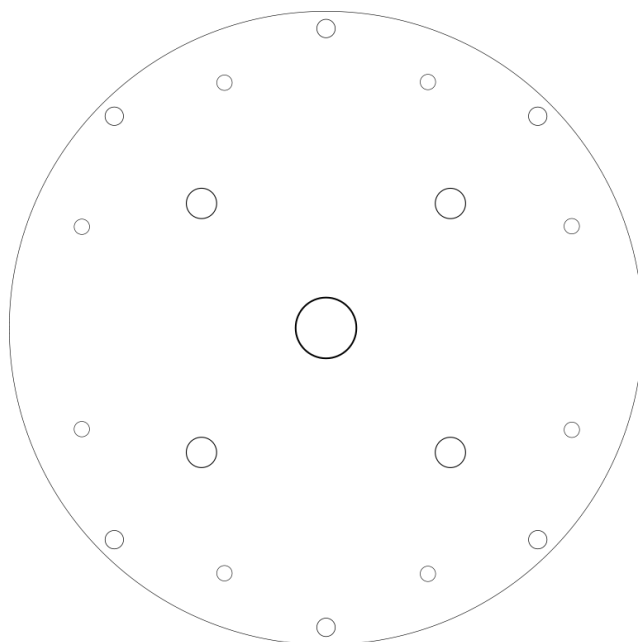
A Plexi-glass design in Inkscape



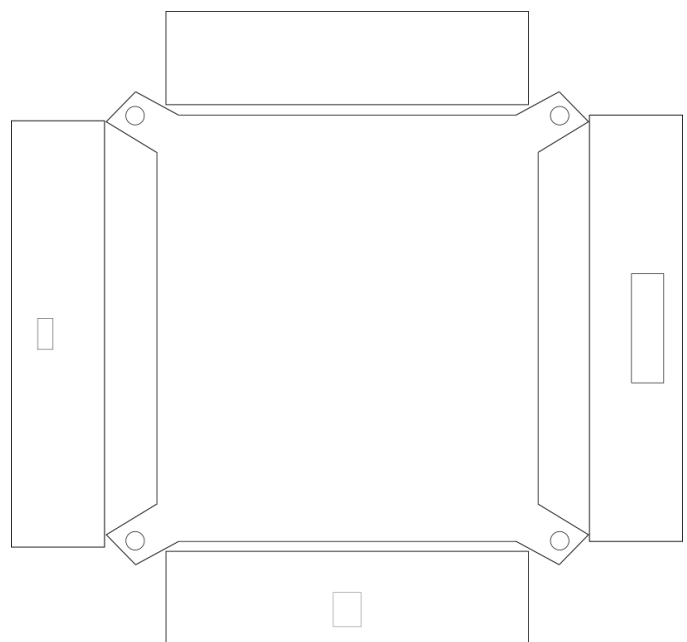
(a) Top plate



(b) Solenoid plate

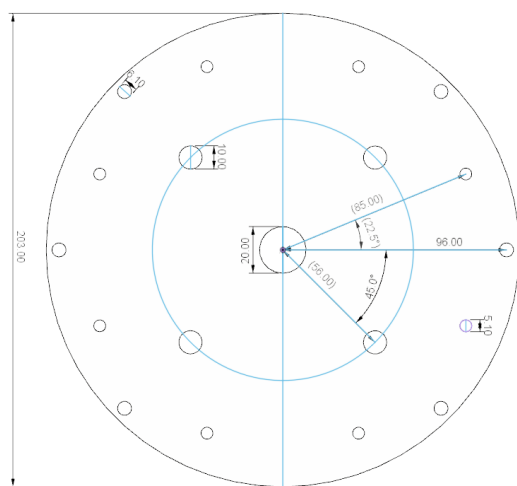


(a) Magnet base

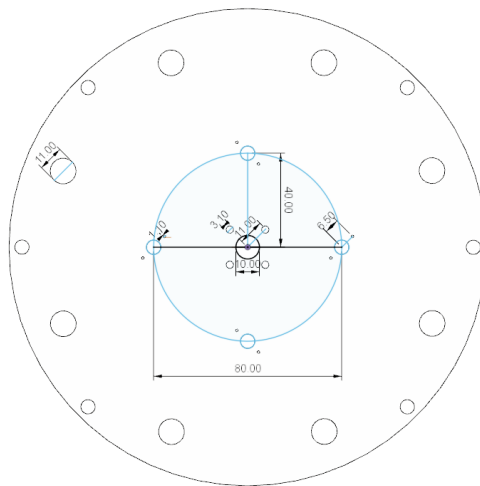


(b) Electrical housing

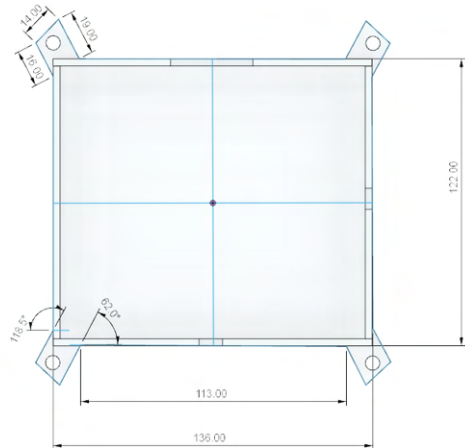
B Plexi-glass design in Fusion360



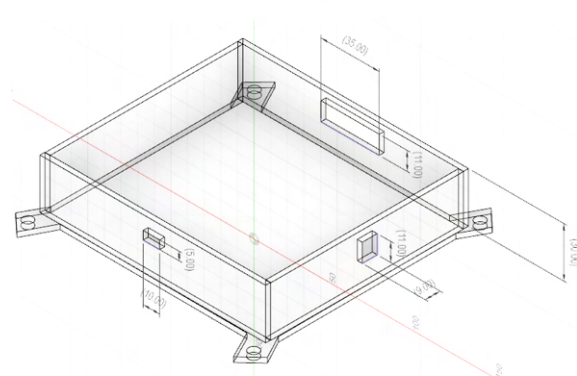
(a) Magnet plate



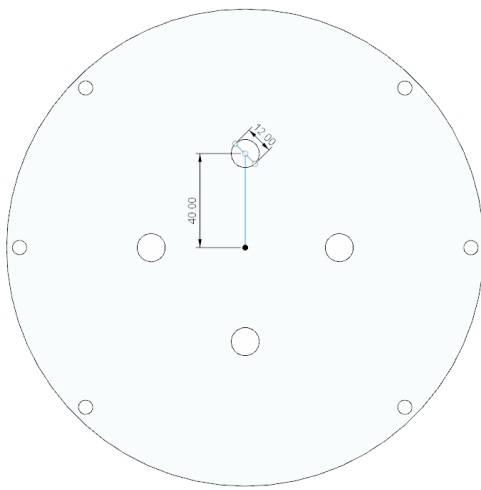
(b) Solenoid plate



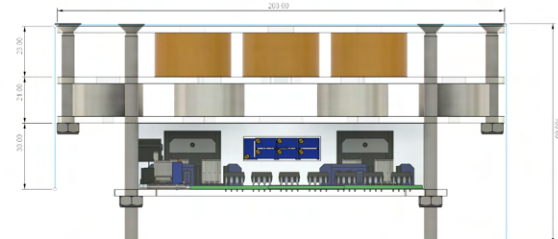
(c) Electrical housing above



(d) Electrical housing side



(e) Top plate



(f) System from side

C Sources for used 3D assets in Fusion360

As per grabCAD licence; <https://grabcad.com/terms> the following models has and can be used for NON-commercial purposes when sources is given:

Potentiometer:

<https://grabcad.com/library/potenciómetro-2>

Jesús A. Pérez Rincón

LM2596 DC-DC StepDown Converter (Buck converter):

<https://grabcad.com/library/lm2596-dc-dc-stepdown-converter-1>

Ivano De Marchi

DS-210 2.1mm DC Female Barrel Jack:

<https://grabcad.com/library/ds-210-2-1mm-dc-female-barrel-jack-1>

Vasily Kashirin

Breadboard 30 x 70 mm:

<https://grabcad.com/library/breadboard-30-x-70-mm-1>

Doctor Rozum

Prototyping Breadboard:

<https://grabcad.com/library/prototyping-breadboard-1>

Gabriel Tóth

Teensy 4.0

<https://grabcad.com/library/teensy-4-0-1>

Simon Nylund

As per snapEDA license; <https://www.snapeda.com/about/terms/> the following models has and can be used for NON-commercial purposes:

INA 128(Instrumental amplifier):

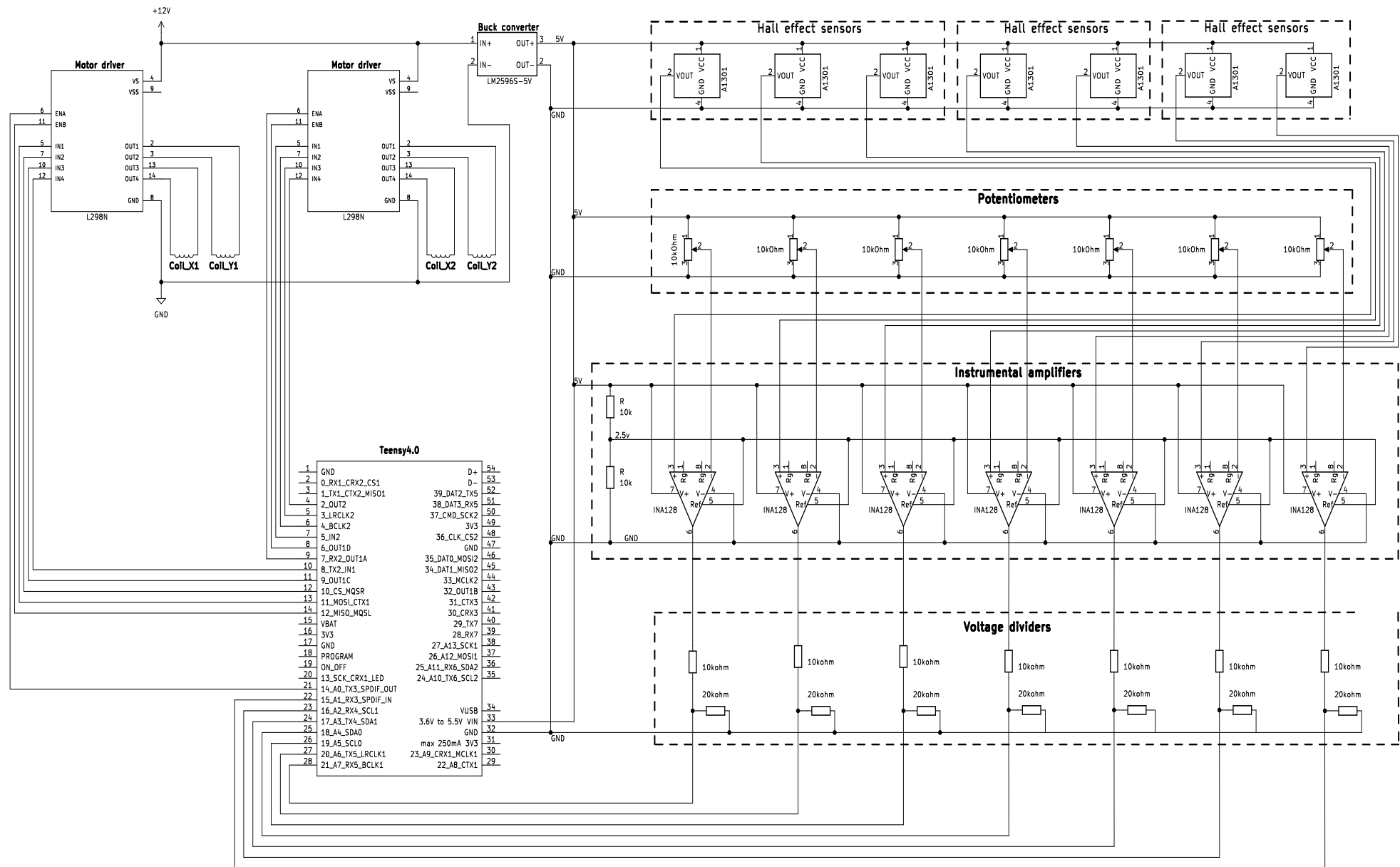
<https://www.snapeda.com/part/INA128PA/Texas%20Instruments/view-part/?company=Nument&t=INA128amp;welcome=homeamp;ref=search>

As per autodesk license; <https://www.autodesk.com/company/legal-notices-trademarks/website-terms-of-use/terms-of-use-english> the following models has and can be used for NON-commercial purposes:

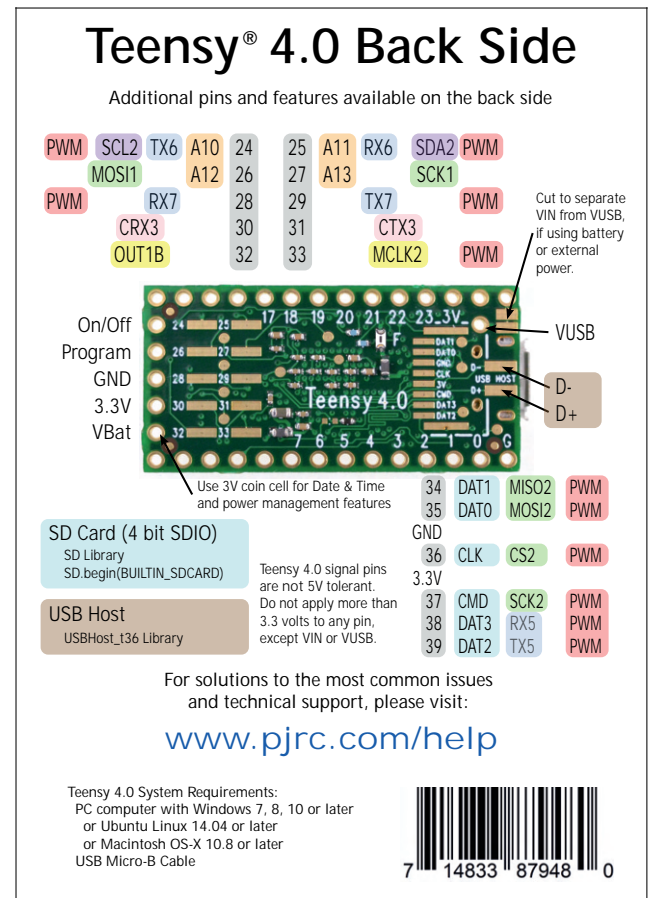
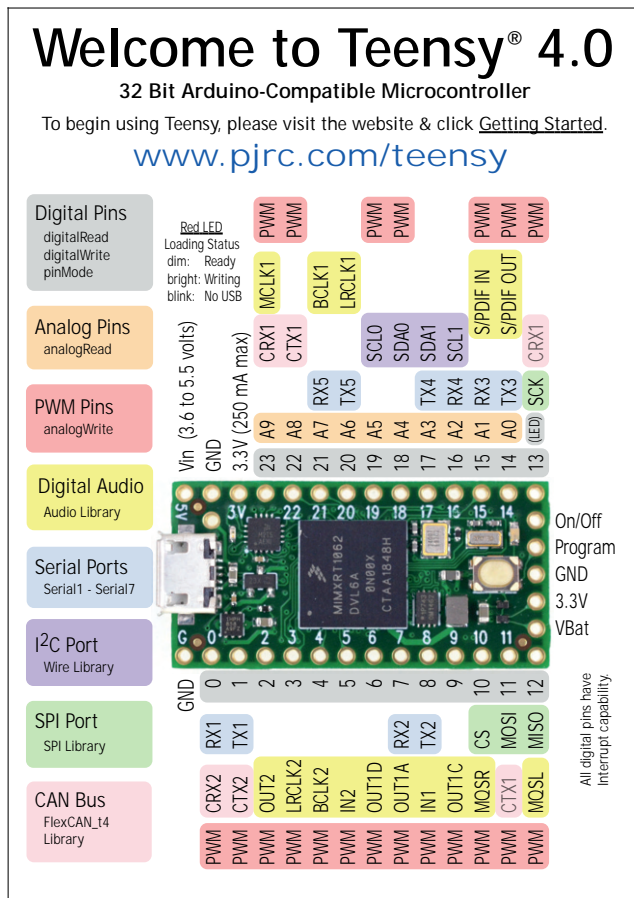
L298N motor driver:

<https://gallery.autodesk.com/projects/133940/l298n?searched=TecnologiasMagallanes+Ies+Magallanes>

D Electrical schematic, landscape



E Teensy Pinout



F Matlab parameters

params	Variable	Description	Value	Unit
solenoids	ri	Inner radius	0.0050	m
	ro	Outer radius	0.0175	m
	h	Height	0.0200	m
	nr	Number of rings in radius	20	
	nh	Number of rings in height	50	
	nl	Number of discretizations	100	
	N	Number of solenoids	4	
magnets	R	Radius of solenoid circle	0.040	m
	zs	Offset along z-axis	0.023	m
	ri	Inner radius	0.0025	m
	ro	Outer radius	0.0160	m
	h	Height	0.0150	m
	nr	Number of rings in radius	20	
	nh	Number of rings in height	25	
levitatingmagnet	nl	Number of discretizations	100	
	N	Number of permanent magnets	8	
	R	Radius of permanent magnet circle	0.085	m
	I	Equivalent current	-43,22	
	offset	Offset angle	0	
	ri	Inner radius	0	m
	ro	Outer radius	0.03	m
sensor	h	Height	0.005	m
	nr	Number of rings in radius	20	
	nh	Number of rings in height	25	
	nl	Number of discretizations	100	
	I	Equivalent current	-9,1	
	m	Mass	0.117	kg
	x	x-coordinates	[0,0,0]	m
sensor	y	y-coordinates	[0,0,0]	m
	z	z-coordinates	[0.004, 0.004, 0.009]	m

G Linearized system matrices

$$A = \begin{bmatrix} & & O_{6x6} & & & I_6 \\ & 195.154 & 0 & 0.012 & 0 & -4.599 & -0.024 \\ & 0.474 & 195.139 & -0.438 & 4.601 & 0.017 & -0.001 \\ & 0.06 & -0.131 & -390.292 & 0 & -0.009 & -0.002 \\ & 0.117 & 20255.365 & -1.031 & -514.903 & 4.53 & -0.94 \\ & -20261.823 & 19.326 & -40.844 & 0.073 & -513.966 & 0.3 \\ & 0 & 0 & 0 & 0 & 0 & 0 \end{bmatrix} \in \mathbb{R}^{12x12}$$

$$B = \begin{bmatrix} & & O_{6x6} & & \\ & -0.014 & -139.148 & -0.016 & 139.343 \\ & -139.297 & -2.089 & 139.463 & -0.392 \\ & -23.659 & -24.321 & -24.191 & -23.806 \\ & -11271.796 & 2.048 & 11270.956 & 0.223 \\ & -73.992 & 11334.028 & 72.371 & -11269.098 \\ & 0 & 0 & 0 & 0 \end{bmatrix} \in \mathbb{R}^{12x4}$$

$$C = \begin{bmatrix} & & & & & \\ & -2.07e03 & 0 & 0 & 0 & -83.61 \\ & 1.27e-13 & -2068.5 & 0 & 83.61 & 5.06e-16 \\ & 0 & 0 & 4.14e03 & 0 & 0 \\ & -2.07e03 & 0 & 0 & 0 & -83.61 \\ & 1.27e-13 & -2068.5 & 0 & 83.61 & 5.06e-16 \\ & 0 & 0 & 4.14e03 & 0 & 0 \\ & -2.96e03 & 0 & 0 & 0 & -126.8 \\ & 1.81e-13 & -2.96e03 & 0 & 126.8 & 1.63e-15 \\ & 0 & 0 & 5.92e03 & 0 & 0 \end{bmatrix} \in \mathbb{R}^{9x12}$$

H Poster

Magnetic Levitation Platform: Design, prototyping and testing of a digital PID-controller

Introduction

Magnetic levitation is a technique used to suspend an object in the air using nothing but magnetic fields. Although most people associate magnetic levitation with high speed trains, the technology also has other uses.

Assignment

The main focus of this project was:

- Designing and building a magnetic levitation platform
- Controlling the position of a levitating magnet using a digital PID controller

This involved designing a system suitable for control, connecting it to a microcontroller and implementing a PID controller. The finished system is meant to be a proof of concept, to possibly be used as a learning platform at ITK in the future.



[1] W Jones. "Earnshaw's theorem and the stability of matter". In: European Journal of Physics 1.2 (Apr. 1980), 85–88. <https://doi.org/10.1088/0143-0807/1/2/004>. (Accessed: 06.05.22). doi: 10.1088/0143-0807/1/2/004. url: <https://doi.org/10.1088/0143-0807/1/2/004>.

[2] R. Doshmanzari, H.A. Engmark and K.T. Hoang. Maglev model description. https://folk.ntnu.no/hansae/Maglev_System_Description.pdf (Accessed: 13.05.2022). 2021.

Theory

One of the most essential theorems in the magnetic levitation industry, is a theorem presented by Samuel Earnshaw in 1840. The theorem states that "no system of charged particles can be in stable static equilibrium in the absence of external forces" (Jones 1980) [1].

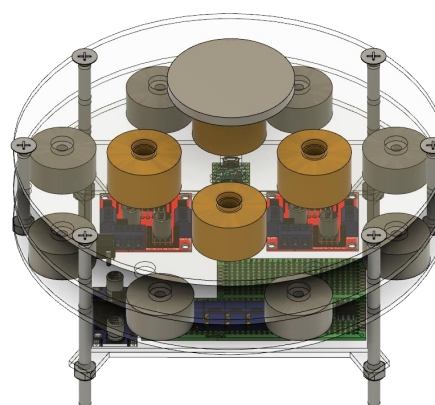
This essentially means that it is not possible to keep the levitating magnet stable, only by the static magnetic field from permanent magnets. The levitating magnet needs some form of stabilizing force, which in this project is provided by four solenoids. The goal is therefore to control the solenoids in order to create a stable equilibrium for the levitating magnet.

The mathematical framework is based on an existing model description (Doshmanzari, Engmark and Hoang 2021)[2] that models an analog system.

All magnets in the system are modelled as solenoids, which again are modelled as thin wire loops. The force on the levitating magnet is computed from the current in the thin wire loops using Biot-Savarts law and Laplace's force law.

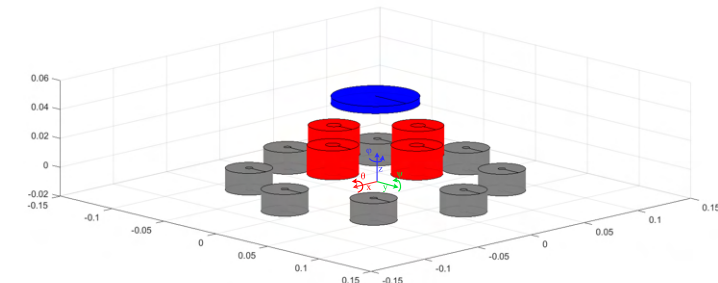
The mathematical framework is implemented as a Matlab model which can be used to simulate the trajectory of the levitating magnet.

The Matlab model was also used to decide what magnet configurations to use.



To determine the position of the levitating magnet, hall effect sensors were used. They do not directly measure the position of the magnet, but rather the change in the magnetic field. This can be used to determine the position of the magnet, by observing the change of the magnetic field caused by the positioning of the levitating magnet. However, the sensitivity of these sensors are too low to be measured normally, an In-Amp is connected to amplify the signal.

During the testing it was discovered that the magnetic fields generated from the solenoids were too weak to control the levitating magnet from the same height as the permanent magnets. Due to that, the physical system was designed to have multiple layers. The bottom layer contains the electronics and the microcontroller. An incremental PID-controller was implemented in the microcontroller.



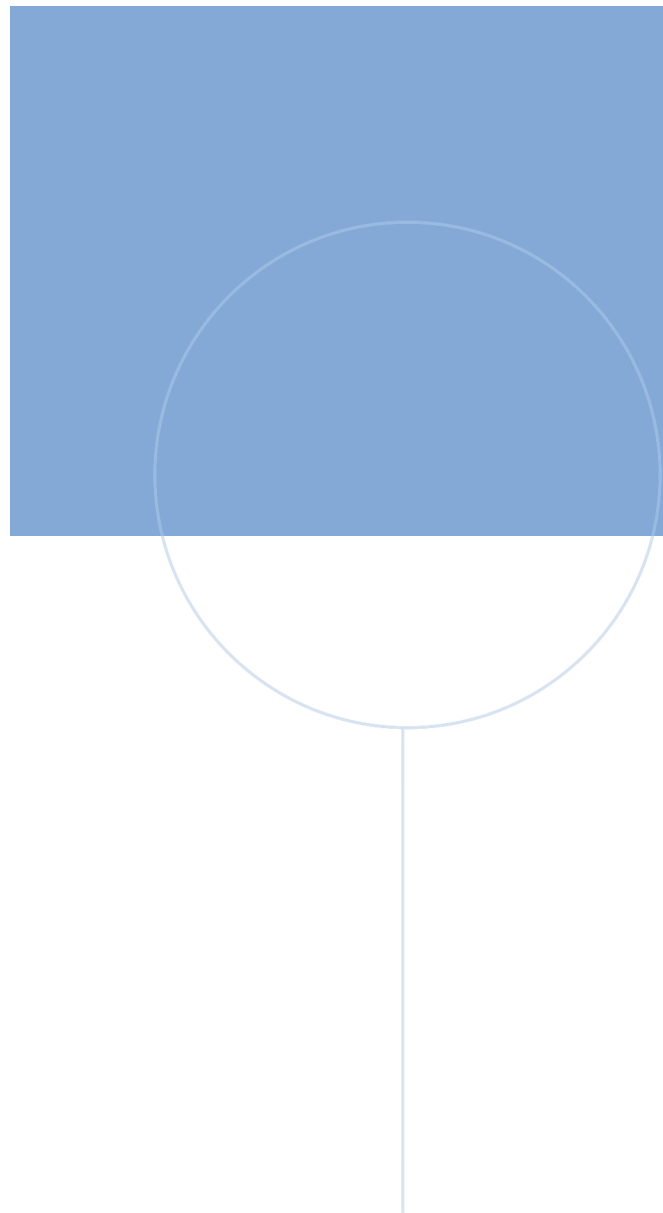
Design

The project produced a functional but unstable magnetic levitation platform. Use the QR-code for a video showing the levitation.

Conclusion

The result shows that the system should be possible to stabilize, given further testing and improvements on the current system





NTNU

Norwegian University of
Science and Technology